1   *U-Th-Pb zircon geochronology by ID-TIMS, SIMS, and laser*

2   *ablation ICP-MS: recipes, interpretations, and opportunities*

3

4

5   U. Schaltegger[1], A. K. Schmitt[2], M.S.A. Horstwood[3]

6   [1]Earth and Environmental Sciences, Department of Earth Sciences, University of Geneva,

7   Geneva, Switzerland (urs.schaltegger@unige.ch)

8   [2]Department of Earth, Planetary, and Space Sciences, University of California, Los Angeles,

9   USA (axel@oro.ess.ucla.edu)

10   [3]NERC Isotope Geosciences Laboratory, British Geological Survey, Keyworth, Nottingham

11   NG12 5GG, UK (msah@nigl.nerc.ac.uk)

12

13

14

15   **Corresponding author:**

16   Urs Schaltegger

17   Department of Earth Sciences

18   Rue des Maraîchers 13

19   1205 Geneva, Switzerland

20   email: urs.schaltegger@unige.ch

21   phone: +41 22 379 66 38

22   fax: +41 22 379 32 10

23

24

25

1

Abstract

The chronologic record encoded in accessory minerals, based on the radioactive decay of U and Th, is indispensable to extract quantitative process rates over timescales encompassing Earth's evolution from the Hadean to the Holocene, and extending from terrestrial to extra-terrestrial realms. We have essentially three different U-Pb dating tools at hand, a high-precision, whole-grain bulk technique (isotope-dilution thermal ionization mass spectrometry, ID-TIMS), and two high-spatial resolution but less precise in-situ techniques (secondary ion mass spectrometry, SIMS, and laser ablation inductively-coupled plasma mass spectrometry, LA-ICP-MS), all of which are predominantly applied to the mineral zircon. All three have reached a technological and methodological maturity in data quality and quantity, but interpretational differences, which are often common (albeit at different temporal and spatial scales) to all isotopic dating techniques, remain largely unresolved. The choice to use one of these techniques should be governed by the scientific question posed, such as (1) the duration of the geological process to be resolved; (2) the size and abundance of the material to be analysed; (3) the complexity of the sample material and of the geological history to be resolved; and (4) the number of dates needed to address the question. Our compilation demonstrates that, ultimately, the highest confidence geochronological data will not only result from the optimal choice of appropriate analysis technique and the accurate treatment of analytical and interpretational complexities, but also require comprehensive sample characterization that employs the full gamut of textural (e.g., cathodoluminescence, charge contrast imaging, electron backscatter diffraction) and compositional (e.g., trace element, stable and radiogenic isotope) analysis.

1. Introduction

Determining timescales of accessory mineral crystallization is critical for deciphering process rates in magmatic and metamorphic environments. Reconstruction of these processes must account for their non-instantaneous or repetitive nature: magmatic cycles can last over several 100 ka (e.g., Claiborne et al., 2010; Schoene et al., 2012) and hydrothermal activity and formation of ore deposits occurs in short events that collectively may last up to several 100 ka as well (e.g., Dalrymple et al., 1999; Chiaradia et al., 2013). Even for geologically young systems, it is, however, often challenging to discriminate between individual and repeated events. Because temporal resolution is inevitably coarser in deep geologic time, multiple high-frequency events are masked by a lack of age resolution and are integrated into quasi-continuous processes or instantaneous "events". Substantial efforts are undertaken to improve precision and accuracy of dating techniques to better meet the requirements of temporal resolution. As a consequence, analytical uncertainties approach the timescales of high-frequency events in magmatic and metamorphic environments and critical questions need to be addressed: What are the limiting factors of geochronological techniques – are they defined by the isotopic system, by the minerals we analyse, or by the analytical equipment we use? Where are the limits for interpreting a date (the numerical result of an isotopic analysis) as an age (the chronologic significance assigned to one or a series of dates) - are they inherent to open or complex isotopic system behaviour, due to our insufficient knowledge of how complex magmatic or metamorphic systems work in nature or is data quality and quantity an issue?

We will first review some recent innovations in both high-precision and high-spatial resolution U-Pb dating represented by chemical abrasion - isotope dilution - thermal ionization mass spectrometry (CA-ID-TIMS), secondary ion mass spectrometry (SIMS), and laser ablation - inductively coupled plasma mass spectrometry (LA-ICP-MS). CA-ID-TIMS represents the highest precision bulk dating method for zircon extracted from volcanic and plutonic rocks, whereas the two high-spatial resolution techniques SIMS (for U-Th disequilibrium dating of young volcanic zircon and for highest-spatial resolution geochronology of magmatic, metamorphic, and diagenetic crystal domains) and LA-ICP-MS (for magmatic, metamorphic, and detrital zircon; see Table 1) have wide applicability where bulk methods are limited by the internal complexity of the sample, by sample size or required data quantity. After summarizing key preparation and analysis procedures of the three U-Th-Pb dating techniques, we will discuss problems of both analytical-technical and

83   interpretational nature that have become obvious with increasing analytical precision and the

84   understanding of process timescales gleaned from the study of active systems. An important

85   aspect of this review is that key problems in interpreting accessory mineral geochronology

86   are often similar or inter-related for the different methods, despite their differences in spatial

87   and temporal resolution. We concentrate on the isotope systems of zircon as the main and

88   most commonly used mineral for dating via the U-Pb decay systems, mainly because of its

89   refractory behaviour throughout many geological processes, as well as the stability of its

90   lattice even under conditions of high temperature and pressure. Other possible targets for U-

91   (Th-)Pb geochronology abound, such as baddeleyite (ZrO_2; predominantly in mafic magmatic

92   rocks), monazite (a light rare earth element [LREE] bearing phosphate; $[LREE]PO_4$), or

93   titanite ($CaTiSiO_5$; ubiquitous in magmatic and metamorphic rocks), but these are only

94   addressed for comparison, being aware that to be comprehensive, one would have to add a

95   long list of these and other minerals found in magmatic, hydrothermal, and metamorphic

96   environments where they are used with variable success and often lower precision than

97   zircon. Ultimately we present working guidelines for the optimal use of the available dating

98   techniques and data quality assurance, based on ongoing research, and provide an outlook for

99   improving zircon geochronology to achieve enhanced reliability for data interpretation in a

100   geologic context.

101

102   2. Current analytical and instrumental status and limitations

103   2.1. Chemical Abrasion - Isotope Dilution - Thermal Ionization Mass Spectrometry
104   (*CA-ID-TIMS)*

105   *2.1.1 Overview*

106   The CA-ID-TIMS technique involves the separation of individual zircon crystals from a rock

107   by either bulk methods or by extraction directly from rock sections. The material is then

108   texturally, sometimes compositionally, characterized, pre-treated by chemical abrasion

109   (Mattinson, 2005), and dissolved. The elements of interest - U, Pb, and (rarely) Th - are

110   separated using chromatographic separation techniques in a very clean environment, and their

111   concentrations and isotopic compositions analyzed by isotope dilution and thermal ionization

112   mass spectrometry techniques (e.g., Parrish and Noble, 2003; Schoene, 2014). This technique

113   yields the most precise and accurate U-Pb dates and is mainly applied to magmatic accessory

114   minerals, predominantly to zircon.

In 2003, the U-Pb geochronology community started the EARTHTIME initiative (Bowring et al., 2005), which comprises more than 200 members from 30 countries and has gained widespread acceptance as a successful way forward to improve accuracy and precision of ID-TIMS U-Pb dating. Within this framework, jointly calibrated tracer and calibration solutions have been distributed to minimize the inter-laboratory bias due to different tracer calibrations (Condon et al., in review) and new software has been made available for the community, offering accurate handling of data and their associated uncertainties (Bowring et al., 2011; McLean et al., 2011b). Inter-laboratory bias exercises have shown that the differences between laboratories using EARTHTIME tracers have been reduced to 0.1% demonstrated by round-robin tests using natural zircon or by repeated analysis of synthetic solutions (Condon, 2005; Sláma et al., 2008).

The mineral-dissolution, isotope dilution technique, also termed "conventional", represents a multi-step procedure, which requires a high degree of control on many parameters to ensure highest data quality. Some of the most critical ones, outlining the most important innovations, will be addressed in the following paragraphs.

2.1.2 Sample pre-treatment by annealing and partial dissolution ("chemical abrasion")

The "chemical abrasion" treatment of selected zircon crystals prior to their dissolution involves annealing at 850-900°C, followed by partial dissolution in HF or HF-HNO$_3$ mixtures (Mattinson, 2005). It now has replaced the mechanical air-abrasion technique used since Krogh (1982). The treatment increases concordancy of ID-TIMS U-Pb dates by efficiently removing zircon domains that have a higher degree of damage due to the radioactive decay of uranium in the crystal, causing potential loss of radiogenic Pb. Chemical abrasion increases precision and reproducibility but preferentially dissolves and removes U-rich zones, thus possibly biasing the result towards the age of the lower-U growth zones. Chemical abrasion may be applied collectively to a group of bulk separated zircon crystals, or individually to single crystals or crystal fragments extracted from an epoxy mount, following imaging and possibly in-situ chemical or isotopic analysis. Chemical abrasion techniques have been tested on some other accessory phases without clear evidence of improving concordance (e.g., baddeleyite, Rioux et al., 2010; monazite, Peterman et al., 2012).

2.1.3 Mass spectrometry

148 Isotope ratio analysis is performed on a thermal ionization mass spectrometer (TIMS), an

149 instrument with a typical mass resolution of $M/\Delta M =$ ~500 at 10% valley definition (Murray

150 et al., 2013). This mass resolution does not allow for resolution of interferences (e.g.,

151 $^{138}Ba^{31}P^{17}O^{18}O$ on mass ^{204}Pb or ^{205}Tl interfering with the synthetic spike isotope ^{205}Pb),

152 which therefore have to be monitored and appropriately corrected using mass 201 (which has

153 a $^{138}Ba^{31}P^{16}O_2$ interference on it) and ^{203}Tl, respectively. Loading Pb onto a Re filament in

154 conjunction with small amounts of a Si-gel activator and phosphoric acid produces long-lived

155 ion beams of high stability that are mostly too small for Pb isotope analysis on Faraday

156 collectors, but require the use of secondary electron or photo-multipliers in ion counting

157 mode (Richter et al., 2001; Palacz et al., 2011). Mass spectrometric sensitivities of ID-TIMS

158 (as well as for SIMS and LA-ICP-MS) are consistently expressed here as "useful ion yield"

159 (or "useful yield" in short) which is defined as the number of detected ions of an isotopically

160 pure species (atomic or molecular) divided by the total number of atoms of that isotope in the

161 analyte mass. For ID-TIMS, the useful yield of Pb ranges between 1.6 and 6.4% using

162 different Si-gels (Gerstenberger and Haase, 1997; Huyskens et al., 2012; Table 1). The best

163 ion yields are generally obtained by depositing a thin layer of Si-gel made from silicic acid

164 (Gerstenberger and Haase, 1997) onto the Re filament. Isotope ratio analysis by TIMS is

165 routinely corrected for mass-dependent fractionation; a non-mass dependent fractionation

166 component affecting the odd-valued ^{203}Tl, ^{205}Pb and ^{207}Pb isotopes has also been reported by

167 Amelin et al. (2005) and McLean et al. (2011a). The U isotope composition is determined as

168 UO_2^+ from the same Si-gel load used for Pb analysis, requiring knowledge of the oxygen

169 isotope composition of the analyte loaded onto the Re filament, to correct for isobaric

170 interference of $^{233}U^{18}O^{16}O$ on $^{235}U^{16}O_2$. UO_2^+ is analysed sequentially in ion counting mode

171 or simultaneously with Faraday cups equipped with 10^{12} Ω resistors. Using Faraday

172 collection at low ion beam intensities requires accurate control of baseline intensity and

173 stability, amplifier gain calibration and resistor decay rate.

174 The uncertainty in Pb isotope ratio determinations is composed of two major components: (1)

175 the pulse counting statistic which is limited by the low ion beam signal measured on an ion

176 counter (% = $1/\sqrt{N}*100$ where N = total number of counts); using multi-collection via an

177 array of multipliers does not improve the precision, but adds the uncertainty of the multiplier

178 cross-calibration to the counting statistics, and (2) the mass fractionation correction inherent

179 to the TIMS source. No uncertainty is usually attached to the empirically determined dead

180   time of the multiplier, despite the well-known day-to-day fluctuations of secondary electron

181   and photo multiplier tubes.

182

183   *2.1.4 Uncertainty, accuracy, data treatment, and error reporting*

184   A good knowledge of the sources of error is a prerequisite for intercalibration between

185   different isotopic and non-isotopic (e.g., astrochronological) geochronologic techniques.

186   Correct uncertainty estimation allows distinction between purely analytical data scatter and

187   externally caused, excess data dispersion. It is also critical to avoid mistaking inter-

188   chronometer bias such as between U-Pb and $^{40}Ar/^{39}Ar$ chronometers (e.g., Renne et al., 2010)

189   for a real age difference. Later, we discuss briefly the different sources of uncertainty and

190   error, a detailed and complete appraisal of which can be found in Schoene et al. (2013).

191   Zircon analyses may contain minute amounts of two types of Pb that are unrelated to U and

192   Th decay: (1) Initial non-radiogenic Pb, commonly referred to as "common-Pb", is

193   incorporated during crystallization. The uncertainty in the isotopic composition of the

194   common lead correction (Pb_{com}) dominates the analytical uncertainty at low Pb_{rad}/Pb_{com}, and

195   mainly affects the $^{207}Pb/^{235}U$ system. The isotopic composition of Pb_{com} may be estimated

196   from the crustal growth model of Stacey and Kramers (1975) or from analysis of U-deficient

197   minerals in the same sample, such as feldspars. Since most analyzed zircons contain very

198   limited amounts of Pb_{com}, the Pb_{rad}/Pb_{com} is mainly limited by the procedural blank. (2)

199   Procedural blank Pb is introduced during chemical separation and analysis and can be

200   distinguished from common-Pb by its different isotopic composition. State-of-the-art

201   procedures may yield blank levels as low as 0.2 pg, including dissolution, ion

202   chromatography and isotope analysis. Such low blanks are a pre-requisite to analyse small,

203   low-U and/or young zircons at high precision. Accurate knowledge of the isotopic

204   composition of the procedural blank component is essential at Pb_{rad}/Pb_{com} ratios <5; the

205   uncertainty on the isotope ratios used has to be propagated onto the final result. The effect of

206   different Pb_{com} (isotopic composition on two zircons with different Pb_{rad}/Pb_{com} ratios is

207   shown in Fig. 1a.

208   *Insert here: Fig. 1*

209   The accuracy of a U-Pb date determined by ID-TIMS is mainly determined by the accuracy

210   of the tracer calibration, as well as by the U decay constant uncertainty. Prior to

211   EARTHTIME, individually calibrated tracer compositions resulted in up to 1% inter-

212   laboratory bias on ^{206}Pb/^{238}U dates; the use of the (^{202}Pb-) ^{205}Pb-^{233}U-^{235}U tracer solutions

213   distributed by EARTHTIME (ET2535 and ET535 tracers, respectively; www.earth-time.org)

214   has now enhanced inter-laboratory reproducibility to better than 0.1% on ^{206}Pb/^{238}U dates.

215   The tracer has been calibrated in different laboratories by using internationally certified,

216   synthetic calibration solutions, and is controlled by analysis of international synthetic and

217   natural reference materials (www.earth-time.org). The mass-dependent fractionation of

218   unknown samples in the TIMS source may be quantified by repeated measurements of an

219   international reference material (SRM 981, 982) but is for high $Pb_{rad.}$/Pb_{com} analyses,

220   preferably quantified and corrected internally by using the EARTHTIME double-isotope

221   tracers for both U and Pb isotopes, taking into account potential isobaric and molecular

222   interference on the two tracer masses ^{202}Pb (^{138}Ba^{31}P^{16}O^{17}O) and ^{205}Pb (^{205}Tl). A continuous

223   control of reproducibility and accuracy has to be established in any laboratory through

224   analysis of synthetic and/or natural reference materials. The EARTHTIME community has

225   started to use synthetic solutions with apparent ages of 10, 100, 500 and 2000 Ma for the

226   assessment of laboratory reproducibility (www.earth-time.org). Reproducibility can be

227   evaluated by repeated analysis of well-characterized natural reference zircons, the most

228   recent (CA)-ID-TIMS ages of which are compiled in Table 2. Repeated analysis of reference

229   materials enables quantification of the long-term reproducibility for an isotope laboratory,

230   and comparing results between different mass spectrometers and different multipliers, the

231   latter requiring exchange every few years (in the case of secondary electron multipliers). An

232   example of a representative dataset of the R33 reference zircon from the University of

233   Geneva lab is shown in Fig. 2, demonstrating the complex nature of analytical work related to

234   (1) poor analytical reproducibility requiring rejection of outliers due to dead time correction

235   problems with the secondary electron multiplier (period 1), and (2) open system behaviour of

236   natural zircon, attributed to insufficient or poorly reproducible chemical abrasion treatment

237   prior to analysis (periods 2 and 3). This also demonstrates the difficulty of discriminating

238   between analytical (multiplier performance) and natural sources (partial open system

239   behaviour) of data scatter. Validation data from synthetic and/or natural materials should be

240   included in any publication that is reporting high-precision U-Pb dates.

241   *Insert here: Fig. 2*

242   Additional factors to take into account are the values for the natural ^{238}U/^{235}U ratio in dated

243   materials (Condon et al., 2010; Hiess et al., 2012) and of uranium decay constants (Schoene

244   et al., 2006; Mattinson, 2010; Boehnke and Harrison, 2014). The latter is accounted for by

245   adding the decay constants' uncertainty band to the concordia curve in all concordia diagrams

246   (Fig. 1). Be aware that for systems older than some 500 Ma, the $^{207}Pb/^{206}Pb$ ratio is the most

247   precisely and reliably dated, at precisions of $\pm$ 0.02% (e.g., Zeh et al., 2015).

248   Substantial discrepancies may be discovered when reducing isotopic data using different

249   software packages, related to different correction and uncertainty propagation procedures.

250   The EARTHTIME community has adopted an integrated open-source software infrastructure,

251   interfaced with commercial mass spectrometers, for read-out and statistical filtering of the

252   raw data ("Tripoli"), followed by a platform allowing for data reduction, correct uncertainty

253   propagation and online data visualization ("UPb_Redux"; Bowring et al., 2011; McLean et

254   al., 2011b). The final uncertainty of a U-Pb date is composed of several random and

255   systematic elements. It is suggested that the community adopts the x/y/z notation proposed by

256   Schoene et al. (2006; 2010a), [x] being the random (analytical) uncertainty, [y] containing the

257   systematic uncertainty of the tracer calibration, while [z] also incorporates the U decay

258   constant uncertainties (Table 1). The [x] uncertainty would be used when comparing data

259   within the same or between laboratories using the same tracer solution, i.e., within the

260   EARTHTIME community, [y] when comparing data based on different tracer solutions, and

261   [z] when comparing U-Pb data with other chronometers such as $^{40}K/^{40}Ar$ (or $^{40}Ar/^{39}Ar$). Such

262   an approach quantifying all random and systematic uncertainties is unfortunately not

263   generally used in geochronology.

264

265   ***2.2 Secondary ion mass spectrometry (SIMS)***

266   *2.2.1 Overview*

267   The unique strength of geochronological SIMS lies in its high spatial resolution and high

268   useful yield or 'sensitivity' (Table 1). These merits result from the extremely shallow

269   emission of target atoms and molecules dislocated by collisions with high-energy primary

270   ions and ejected from a depth within a few nm of the surface. Ejected components include

271   atoms from the target, the primary beam, and other sources (e.g., conductive coating, surface

272   contaminants, residual gases in the vacuum). In-situ ionization of some of these species under

273   ultrahigh vacuum conditions permits efficient ion collection. The high sensitivity of SIMS

274   makes it the least destructive of the three analysis techniques described here, with the

275   advantage that sufficient material is typically preserved to permit post-analysis geochemical,

276   structural, or textural characterization. The flipside of the slow removal of material via

277 sputtering (e.g., sputter rates for zircon are ~0.07 μm^3/sec/nA O$^-$ at lateral beam dimensions

278 of ~2 to 30 μm in diameter and beam intensities of ~50 pA to ~100 nA; Fig. 3) are

279 comparatively long analysis durations required to integrate sufficient counts, typically

280 employing electron multipliers in mono- or dynamic multi-collection. Individual spot

281 analyses may thus last at least several minutes, although 5 s duration rapid screening

282 protocols have been successfully applied to Hadean zircons (Holden et al., 2009).

283 Consequently, SIMS is optimal for dating "valuable" zircons and/or small-volume samples

284 whereas high throughput detrital zircon needs are much better served by LA-ICP-MS.

285 Since the early 1970's, U-Th-Pb zircon analysis has become a routine geochronological

286 application in many SIMS labs worldwide, with an expanding, yet mostly non-routine,

287 spectrum of applications targeting other U-Th-Pb bearing minerals (e.g., apatite, allanite,

288 baddeleyite, calcite, monazite, opal, perovskite, pyrochlore, rutile, titanite, uraninite,

289 xenotime, or zirconolite). U-Th-Pb geochronology has overwhelmingly been the domain of

290 large magnet radius mass spectrometers (SHRIMP, CAMECA ims1270/1280) that have the

291 mass resolution required to resolve the complex mass spectrum resulting from sputtering

292 materials without prior chemical purifications (cf. section 3.4). These instruments are

293 operated by relatively few university or government agency labs, and frequently are

294 employed to serve other demands besides geochronology such as stable isotope analysis.

295

296 *2.2.2 Sample preparation requirements and analysis types*

297 Traditional SIMS mounts are rounds 25.4 mm in diameter, not exceeding ~5 mm in thickness

298 (Fig. 3). The useful area, however, is smaller (diameters of ~22 mm for SHRIMP and of ~20

299 mm for CAMECA) because the lip of the sample holder covers part of the mount and the step

300 between the mount surface and the holder edge causes local distortions in the secondary ion

301 extraction field. Bias in U-Pb elemental fractionation has been reported if targets are located

302 too close to the edge (e.g., Stern and Amelin, 2003). More recently, 35 mm diameter mounts

303 with larger analyzable surface areas and reduced isotopic fractionation near the mount edges

304 have been developed (Ickert et al., 2008; Peres et al., 2012).

305 *Insert here Fig. 3.*

306 In most cases, separated crystals from a rock sample and reference materials are cast in

307 epoxy, or pressed into a soft metal (e.g., indium) to make a mount that can be accommodated

308 in the ion probe sample holder. It is a critical requirement for SIMS that sample surfaces are

309 perfectly flat, requiring euhedral crystal shapes for pressed crystals, or careful grinding and

310 polishing. Moreover, the sample surface needs to be conductive, which is typically achieved

311 by applying a high-purity Au coating. Sectioned grain mounts (Fig. 4) must be imaged prior

312 to analysis to aid in targeting homogeneous domains in complex crystals (see section 4.1). *In-*

313 *situ* analysis (within petrographic thin section) is accomplished by extracting regions of

314 interest using a diamond drill or saw and mounting them together with pre-polished reference

315 zircons. Because sample chambers in SIMS instruments can only hold one mount at a time,

316 the practice of mounting standards closely spaced with the unknowns is highly recommended

317 because every sample exchange may change the analytical conditions (e.g., by altering

318 sample chamber vacuum, temperature, or the extraction potential).

319 *Insert here Fig. 4*

320 SIMS depth profiling takes advantage of the shallow emission of secondary ions, whereby

321 atomic mixing and knock-on scrambles the target to several nm depth, depending on impact

322 energy, angle, primary ion species, and target material (Hunter, 2009). Within these limits,

323 changes in the secondary ion signal can be directly related to compositional variation with

324 depth, once sputter equilibrium is achieved. To better discriminate against secondary ions

325 contributed from the more slowly sputtered edges of the pit, the primary ion beam can be

326 rastered or defocussed and secondary ions gated either electronically or (in CAMECA ims

327 "ion microscope" instruments) through an aperture in the secondary ion path so that ions

328 emitted from the center of the crater are preferentially detected. For meaningful

329 geochronological depth profiling, the sample surface must be flat, and growth domains must

330 be oriented perpendicular to the direction of sputtering and have lateral dimensions larger

331 than the sampled region of the crater. Zircon lends itself to depth profiling because euhedral

332 crystals can be aligned with (100) or (110) prism faces flush with the mount surface (Fig. 4),

333 making it possible to date very thin magmatic, metamorphic, or diagenetic overgrowths on

334 crystal surfaces. For many geochronology applications, in particular for dating young

335 crystals, secondary ion signals need to be integrated to depth intervals larger than the

336 theoretical achievable resolution to obtain meaningful age precision. Nevertheless, sub-µm

337 depth resolution for analysis of zircon growth domains is possible, permitting unique insights

338 into the timescales of magmatic or metamorphic crystallization (see section 4.2).

Scanning ion imaging (SII) is a third type of analysis where 2-D, or, if sequentially recorded images are stacked, 3-D isotopic mapping is achieved (Fig. 4). Lateral resolution is dependent on the size of the primary ion beam which is at a minimum between ~500 nm and 2 μm in diameter for Cs^+ (Ga^+) and O^- primary ion beams, respectively (e.g., Harrison and Schmitt, 2007), and ~10's to 100's nm for NanoSIMS (e.g., Hofmann et al., 2009). Because small primary beams correspond to low secondary ion intensities, SII analyses are generally applied to highly radiogenic samples, for example to localize ~100 nm-sized patches of unsupported high $^{207}Pb/^{206}Pb$ in Archaean zircon (Kusiak et al., 2013; cf. Valley et al., 2014). SII is also applied to augment other imaging techniques used to characterize zonation in the target material (e.g., backscattered-electron BSE or cathodoluminescence CL). Compared to BSE or CL imaging, SII has the advantage that it has the sensitivity to quantify trace element distributions (e.g., for Ti-in-zircon; Hofmann et al., 2009).

Direct ion imaging (DII) is a semi-quantitative technique available in CAMECA ims instruments (Fig. 4). Secondary ions are projected onto a stacked detector consisting of an ion-sensitive channel plate and an electron-sensitive phosphorescent screen. In DII, spatial resolution relates to aberrations in the secondary ion transmission (typically ~0.5 μm), and is thus independent of the primary beam dimensions. A practical application of DII is aiding primary beam targeting for small targets that are not readily visible in the optical (reflected light) imaging or establishing isotope or elemental maps of a sectioned mineral.

2.2.3 Inter-element ratio calibration: procedures and sources of bias

Pb-isotopic fractionation in SIMS was found to be largely insignificant, although a subtle instrumental mass fractionation (on average +0.70±0.52 ‰) has been reported for $^{207}Pb_{rad}$ /$^{206}Pb_{rad}$ in zircon (Stern et al., 2009). Consequently, uncertainties for $^{207}Pb/^{206}Pb$ dates are predominantly determined by counting statistics, and assumptions regarding common-Pb (section 2.2.4). In contrast, useful yields for Pb and U species vary strongly, as a rule of thumb for zircon between ~1 % for Pb^+ and UO^+, and ~0.1-0.2% for U^+ and UO_2^+ (note that Pb-oxides are practically absent). This requires a correction based on the calibration of relative sensitivity factors (RSF) using reference materials (e.g., Table 2). Moreover, the Pb^+/U^+ RSF co-varies with the relative abundance of U-oxide species which has long been harnessed to improve the Pb/U RSF calibration by determining working curves involving ratios of U atomic and oxide species (i.e., "two dimensional" calibrations reviewed in detail

by Ireland and Williams, 2003). Regardless of the preferred calibration model, the resulting ~1-3% (2σ) laboratory reproducibility of Pb/U RSF measurements on reference materials believed to be homogeneous (e.g., Jeon and Whitehouse, 2014) frequently exceeds that expected from counting statistics, and is a limiting factor for more precise SIMS analysis. In contrast, the RSF for ThO_x/UO_x (with x = 0,1, or 2) is much closer to unity, typically between 0.9 (e.g, zircon; Reid et al., 1997) and 1.1 (e.g., allanite; Vazquez and Reid, 2004), and thus can be directly determined with a high level of confidence without resorting to a two dimensional calibration.

To accurately apply the Pb/U RSF calibration, it must be realized that compositional differences between reference materials and unknowns can cause RSF variations (the so-called "matrix effects") which, if unrecognized, can lead to systematic errors for the unknowns. It is therefore paramount that reference materials and unknowns compositionally match as closely as possible. This is straightforward for minerals with simple stoichiometry (e.g., zircon, baddeleyite, or rutile), with the possible exception of high-U zircon (e.g., White and Ireland, 2012) and baddeleyite (Li et al., 2010). Minerals other than zircon (e.g., monazite) often show strong compositional variability and require careful matching between reference materials and unknowns (e.g., Fletcher et al., 2010). The analysis of high-energy secondary ions (at -20 to 30 eV offset) mitigates Pb/Th matrix effects for monazite, but comes at the expense of an order-of-magnitude decrease in useful ion yield (Hietpas et al., 2010).

Where correlations exist between U-Pb dates and U abundances, they appear to be related to radiation damage and metamictization because U-Pb determinations of young high-U zircon lacks a concentration bias (White and Ireland, 2012). These findings also support the long-held notion that intact crystallinity of the target zircons is a prerequisite for reliable SIMS geochronology (Ireland and Williams, 2003). The magnitude of the matrix effect has been described as instrumentation and tuning dependent (White and Ireland, 2012), but is broadly similar for different instrumental designs (Fig. 5). High-U zircons also display wider ranges in ion ratios used for calibration (e.g., UO^+/U^+) compared to reference materials with normal-U concentrations (e.g., Temora), but differences exist in the calibration behaviour of high-U and normal-U concentration reference materials on different instruments (Fig. 5). Regardless of these differences, unusual calibration parameters are often a first-order indication of problematic target zircons, and it is therefore recommended to always report the calibration parameters for references and unknowns.

405   A second cause of calibration bias can result from variable ion yields as a function of the

406   crystal orientation with respect to the incoming primary ion beam. These are known as

407   "crystal orientation effects" and have been documented for baddeleyite (Wingate and

408   Compston, 2000) and rutile (Taylor et al., 2012; Schmitt and Zack, 2012), but are not

409   detectable for zircon and monazite (e.g., Wingate and Compston, 2000). Elevated oxygen

410   surface concentration induced by a gas jet (O_2 flooding) pointing towards the sample surface

411   demonstrably mitigates crystal orientation effects for baddeleyite and rutile (Schmitt et al.,

412   2010; Li et al., 2010; Schmitt and Zack, 2012), while also boosting Pb^+ ion yield of the

413   CAMECA ion probes (Schumacher et al., 1994; Schmitt et al., 2010; Schmitt and Zack,

414   2012).

415   A common characteristic of any Pb/U RSF miscalibration, regardless of its origin (e.g.,

416   matrix or crystal orientation effects), is that it shifts data along a trajectory indistinguishable

417   from modern day (Pb-loss) or reverse (U-loss or unsupported radiogenic Pb) discordance. As

418   a consequence, miscalibration causes displacement of the analyses of old zircon at a steep

419   angle to concordia. In the case of reverse discordance, this is readily identifiable as an

420   analytical artefact. When young minerals are dated, instrumental bias introduces variation in

421   U/Pb tangential to the slope of concordia which is more difficult to recognize as an artefact

422   because it resembles minor Pb-loss or inheritance.

423

424   *2.2.4. Common-Pb correction*

425   Common-Pb corrections are critical in SIMS because of the small volume of material

426   consumed which render Pb analyses vulnerable to surface contamination (especially affecting

427   the accuracy of $^{207}Pb/^{235}U$ ages). The presence of non-radiogenic Pb (Pb_{com}) also causes

428   displacement of data points off concordia, but their trajectory is controlled by the

429   composition of $^{207}Pb_{com}/^{206}Pb_{com}$ (Fig. 1). Proxies for common-Pb (primarily ^{204}Pb) typically

430   show decreasing intensities with sputtering time, indicating that most non-radiogenic Pb is

431   surface derived. At UCLA anthropogenic $^{207}Pb_{com}/^{206}Pb_{com} = 0.8283$ (Sanudo-Wilhelmy and

432   Flegal, 1994) is the default Pb composition for correcting zircon where common-Pb intrinsic

433   to the crystal lattice is extremely low. Measures of common-Pb used to determine corrections

434   are ^{204}Pb (stable), ^{207}Pb (quasi-invariant for young zircon; Baldwin and Ireland, 1995), or

435   ^{208}Pb (quasi-stable for zircon with high U/Th; Compston et al., 1984). The main causes for

436 erroneous common-Pb corrections are over- or undercounting of the monitor common-Pb

437 species, in particular for ^{204}Pb. Undercounting can occur if peaks are mis-centered which can

438 typically be avoided by using nearby reference masses for peak centering (e.g., ^{94}Zr$_2$O for

439 ^{204}Pb). Overcounts can result from interferences that are unresolved at the mass resolution

440 M/ΔM = ~4500 at 10% valley definition routinely used for SIMS U-Th-Pb geochronology.

441 Practically unresolvable interferences with their nominal mass resolution requirements in

442 parenthesis are: ^{204}Hg$^+$ (500,000), ^{232}Th^{144}Nd^{16}O$_2$$^{++}$ (50,000), or ^{186}W^{18}O$^+$ (11,000). With the

443 exception of ^{204}Hg$^+$ (sometimes due to contaminated Au targets used for applying the

444 conductive coating), these interferences are much more detrimental for monazite (high Th)

445 and rutile (high W) than for zircon. For monazite and rutile, peak-stripping from monitoring

446 related species (e.g., ^{202}Hg$^+$, ^{232}Th^{144}Nd^{16}O$_2$$^{++}$, or ^{183}W^{18}O$^+$, respectively) or the suppression

447 of the interference using energy filtering can mitigate their impact on the common-Pb

448 correction.

449

450 *2.2.5 Data treatment and error reporting*

451 No universally accepted protocol for SIMS data reduction exists, and software is generally

452 tailored to the specific instrumentation operated by different labs. The diverse types of data

453 (e.g., spot analyses, depth profiles, or ion imaging) further complicate standardized data

454 reduction and reporting. In addition to the considerations about error hierarchies for ID-

455 TIMS, uncertainty reporting for SIMS U-Pb ages requires an additional level because of the

456 dependency on reference measurements and their analytical (random) and systematic

457 uncertainties. Although age is primarily not a factor known to constitute calibration bias

458 because Pb is characteristically present as a trace element below the levels that would cause

459 matrix effects, it is highly recommended to analyze secondary zircon references of similar

460 age as the unknowns under the same analytical conditions. This permits monitoring potential

461 analytical artefacts (e.g., peak misalignments), and aids in constraining an adequate number

462 of points analyzed for the RSF calibration curve whereby reference analyses should bracket

463 the unknowns. Reporting dates for secondary references is thus a recommended practice

464 which permits a first order assessment of data precision and accuracy.

465

466 **2.3 Laser Ablation Inductively Coupled Plasma Mass Spectrometry (LA-ICP-MS)**

467 *2.3.1 Overview*

With the first laser ablation U-Th-Pb dating studies being published ca. 20 years ago (e.g.
Fryer et al. 1993, Feng et al. 1993), this technique is relatively new compared to TIMS and
SIMS geochronology. Since these early studies, the major strength of the technique has been
recognized in its flexibility and speed of data acquisition, making it ideally suited for studies
requiring large datasets such as detrital mineral provenance (e.g. Machado & Gauthier, 1996;
Pullen et al., 2014, and references therein) and detailed investigations into complexly zoned
crystals (Gerdes and Zeh, 2009; Bosse et al., 2009). LA-ICP-MS can be applied to virtually
any U containing material suitable for geochronology (apatite, allanite, baddeleyite,
carbonate, monazite, rutile, titanite, uraninite, xenotime, zircon, and others), with the key
limitation being the availability of homogeneous reference materials (e.g., Table 2). The
method offers high lateral spatial resolution similar to SIMS, with typical spot sizes of 25-35
µm used for zircon geochronology, up to 50 µm for rutile work (having lower average U
concentrations), and as small as 5 µm (though usually 10-15 µm) for monazite dating which
is best performed *in situ* (in petrographic thin sections) to preserve the textural context of the
mineral and its interpretation relative to other structural and geochemical information. Depth
penetration during laser ablation is much higher than during SIMS analysis (see section
2.2.2), with ablation rates usually ranging from 0.35 to 1 µm/sec (0.07-0.1 µm/pulse;
depending on the fluence used) and total crater depths of 15-40 µm during a 30-60 sec
analysis. These lower penetration depths are achievable routinely with higher yielding
instruments and analytical set-ups and recent studies and techniques are pushing even these
limits to shorter durations and lower analyte volumes, (e.g. Cottle et al., 2009, 2012; Johnston
et al., 2009; Steely et al., 2014) including depth profiling with resolution on the order of 150
nm/pulse for a 1-2 µm deep ablation.

The field of LA-ICP-MS has been rapidly expanding, driven by recent major technological
improvements in laser as well as ICP-MS instrumentation and the huge and still growing
demand for dates on magmatic and detrital zircon. One thousand U-Pb analyses per detrital
sample can now be collected efficiently (Pullen et al., 2014) and trace element (or other
isotope) data can be collected from the same volume of material (see discussion in section
4.3). Several recent comprehensive reviews and workshop volumes have summarized the
technical advances in the fundamental understanding of laser-sample interaction (laser
wavelength and pulse width), particle transport issues (sample cell design and carrier gas),
improvements in ion yield and reduction of elemental fractionation by modifications to
carrier and auxiliary gases (e.g. Koch and Günther, 2011; Russo et al., 2013). The LA-ICP-

MS U-Th-Pb community has implemented these recommended improvement strategies for increasing ion yield, reducing laser-induced elemental fractionation and reducing ablated volume, in order to improve data quality. Currently the method limit is stuck at 2% (2σ) for $^{206}Pb/^{238}U$ (Košler et al., 2013) and approximately 1% (2σ) for $^{207}Pb/^{206}Pb$, reflecting inter-laboratory and methodological differences in the generated data (Hanchar, 2009; Košler et al., 2013). However, these limits have been the focus of the laser ablation community over recent years and it has been recognized that more consistent and better documented practices are needed to resolve their origin. Community derived recommendations for better practice have recently been described (see www.Plasmage.org; Bowring et al., 2013).

2.3.2 Laser system influences

Ablation Cell design: Possibly the most significant improvement to have impacted LA-ICP-MS U-Th-Pb geochronology in recent years is the recognition of the importance of ablation cell design on the acquired data. Two-volume cell designs are now standard in most commercial laser ablation systems improving ablation signal response time and profile, consistency of elemental signal and ratio quantification, signal-to-noise ratio and ultimately, precision of data (Müller et al., 2009). Ablation takes place within an inner cup with a smaller effective volume than the larger sample chamber and better controls the local gas dynamics, evacuating the ablated material more efficiently. Signal responses and gas flows across the larger sample chamber are harmonized, providing more consistent inter-element data, particularly important when reference materials are mounted separately to samples. These improved performance metrics have reduced the total ablation duration required and translate directly to improved spatial resolution in area but particularly in depth.

Laser wavelength and pulse width: A second major improvement in recent years has been the more universal adoption of the deep-ultraviolet wavelength (193 nm) laser ablation systems, providing better absorption of the laser energy by the materials of interest, resulting in cleaner and more reproducible ablations, producing smaller particles of more uniform size distribution. These smaller particles (<150 nm) ionize more effectively in the plasma improving signal response, signal and plasma stability, and repeatability of the analyses (Guillong et al., 2003). Recent developments have also seen a move towards using ca. 100 femtosecond pulse widths (Horn and von Blanckenburg, 2007, Koch et al., 2006, Shaheen et

al., 2012) rather than the more traditional 4-25 nanosecond pulse widths, in an effort to improve laser induced inter-element and isotopic fractionation. However, this has not yet shown significant improvement for U-Th-Pb data (d'Abzac et al. 2011; Koornneef et al. 2012) although the optimum wavelengths and pulse widths of femtosecond laser systems used for U-Pb dating have yet to be established.

2.3.3 Mass Spectrometry

Multiple collector (MC)-, single collector (SC)- and quadrupole (Q) ICP-MS are employed for U-Pb geochronology and achieve broadly the same results, at least with respect to the limiting Pb/U uncertainty. Some improvements in Pb isotope data can be achieved using MC-ICP-MS but newer very rapid scanning SC-ICP-MS instruments can achieve similar counting statistic precision, limited only by the dynamic range of the multiplier, due to their pseudo-simultaneous mode of operation. However, until improvements of the limiting Pb/U uncertainty can be realized, improved Pb isotope precision of one form of MS over another is of limited value since resolving concordance is constrained by the larger Pb/U uncertainty. Ultimately, single-collector detection will always be less precise than multi-collector detection for highly variable, low intensity and/or short duration ion beam signals even for the fastest scanning mass spectrometer systems. This is due to counting statistic limitations resulting from the short dwell times required during rapid scanning mass spectrometry and the non-simultaneous acquisition of the isotopes during rapid signal variations (spectral skew). However, more practical limitations complicate the optimal choice of ICP-MS for laser ablation analysis. For most routine U-Pb applications, a Q-ICP-MS system can achieve the same Pb/U uncertainties as the sector field instruments due to the laser ablation and ICP-based limiting uncertainties being greater than any spectral skew contributions when appropriate analysis routines are selected. However, this comes at the expense of greater sample consumption due to their lower ion yields, causing compromise in the spatial resolution of the analysis. Q-ICP-MS systems are also less able to reliably measure the low level ^{202}Hg and ^{204}(Pb+Hg) peaks required for the correction of common-Pb. MC-ICP-MS systems are constrained by their limited dynamic range in their ion counting systems. Here, ion beams not much more than 1M cps (or those expected to reach this level in a small amount of time) cause protection mechanisms to 'trip' into place, ending the acquisition and generally causing loss of that analysis. Lower yielding SC-ICP-MS instruments are better

564 equipped to deal with such dynamic range variations by utilising quadrupole-like dual

565 detection systems that switch rapidly from the pulse counting to analogue conversion range

566 of the detector, thereby continuing the analysis. However, the calibration of this switch

567 between the dual detection modes requires care to achieve accuracy and contributes an

568 uncertainty usually in the percent range.

569 Great strides have been made in improving 'sensitivity' of mass spectrometers, coupled with

570 the improvements in cell geometry mentioned above. The quotation of instrumental

571 "sensitivity" varies across the ICP-MS community depending on what type of ICP-MS is

572 being used (e.g. MHz or GHz per ppm concentration for SC and Q-ICP-MS, Volts per ppm

573 concentration for MC-ICP-MS). However, all of these approaches require knowledge of the

574 amount of material utilised to allow them to be compared. In the same way, signals derived

575 by laser ablation on one instrument cannot be compared with another (or even between

576 analyses from the same set-up on two different days), unless an ablation rate or total ablation

577 pit volume is known.

578 Instrumental 'sensitivity' expressed as useful yield is independent of the method used to

579 collect the data (Table 1). It is suggested that this be a new standard (*sensu stricto*) for

580 reporting ICP-MS instrument performance with respect to signal response. Determination of

581 nebuliser uptake rate is all that is required for solution analyses, with laser ablation analyses

582 requiring determination of ablation rate per pulse at a particular laser fluence for a given

583 mineral. Expressed in this way all ICP-MS instruments can be compared within and between

584 laboratories, in wet plasma or dry, solution introduction or laser ablation, and compared to

585 equivalent SIMS and ID-TIMS metrics for a much more informative evaluation. Typical

586 useful yields for different instrument types are shown in Table 1 and better highlight their

587 differential capabilities whilst noting that although similar yields might be achieved (e.g.

588 SIMS; c.f. TIMS), the amount of material sampled constrains the overall achievable data

589 precision. Hence, TIMS data are more precise than SIMS despite having equivalent yields

590 and ICP-MS data can be as precise as SIMS but at the sacrifice of volume, despite having

591 lower useful yields. For the best precision at the smallest volume though, nothing currently

592 betters SIMS due to its comparatively high useful yields and small sampling volume.

593

594 *2.3.4 Source of bias and overall uncertainty*

595   One of the fundamental controls on U-Pb fractionation during laser ablation is the fluence

596   used for ablation. Greater fluence ($J.cm^{-2}$) results in more ablation and therefore greater

597   downhole fractionation of the measured Pb/U ratio. The ability to correct this and the

598   uncertainty assigned to that correction, relies on the consistency of this fractionating profile.

599   In a homogenous material, therefore, the consistency or repeatability of the laser fluence is

600   critical to obtaining reproducible U-Pb data. As the community targets reduction of the U-Pb

601   uncertainty, laser fluence repeatability and therefore fluence-induced Pb/U variation, will

602   also need to improve. With increasing emphasis on single pulse, pulse-to-pulse and short

603   ablation data analysis, laser fluence repeatabilities will need to be tightly constrained if they

604   are not to become limiting to the achievable uncertainty. Ideally, it might be expected that the

605   variability of Pb/U as a result of fluence repeatability, should be ten times lower than the

606   overall target uncertainty to limit the impact of this parameter.

607   Laser-induced inter-element (or down-hole) fractionation (LIEF) is still one of the limiting

608   analytical factors in LA-ICP-MS U-Pb dating. Combined with metamictisation, geochemical

609   and structural alteration (of zircons and other accessory phases) affects the ablation rate of

610   the material, varying LIEF within and between materials of the same nominal composition.

611   This results in systematic inaccuracies in the determined sample or validation results when

612   directly compared to a reference material. Since these structural and geochemical variations

613   naturally occur, this effect can only be mitigated by reducing the degree of LIEF occurring in

614   the first place. This principally requires the use of low laser fluence and/or larger spot sizes to

615   prevent excessive depth penetration and restrict the aspect ratio of the ablation pit to less than

616   1:1, that is, a depth less than the spot size. This is more easily achieved therefore, by more

617   'sensitive' or efficient set-ups which achieve greater ion yields. The laser hardware and its

618   specific optical design also impact the extent of LIEF and poor gas dynamics in the ablation

619   cell and transport tubing can mask and overprint the true form of the LIEF, complicating its

620   correction. Great care is therefore required to prevent these effects and to limit the degree of

621   LIEF occurring.

622   One of the key problems for LA-ICP-MS U-Pb geochronology is the inability to precisely

623   measure ^{204}Pb for the correction of common-Pb. Despite the time sacrifice (for SC & Q-ICP-

624   MS systems) in doing so, we would like to advise that the two principal masses ^{202}Hg and

625   ^{204}(Pb+Hg) should be monitored in any case, even imprecisely, to allow recognition of

626   common-Pb components clearly above background. Without this, the cause of discordant

627   data points can only be surmised to be common-Pb rather than demonstrated. Ultimately

628 however, laser ablation is limited in its ability to correct for common-Pb when compared to

629 both ID-TIMS and SIMS. Equally, 'blind acceptance' of common-Pb corrected data, without

630 scrutiny of the data scatter prior to correction, can mislead interpretations due to masking of

631 non-analytical scatter by the increased data point uncertainties after correction. In addition,

632 false impressions of concordance may result as data are forced to the concordia by assuming

633 potentially inaccurate common-Pb compositions for correction. This is potentially a problem

634 at all scales of precision for each of the techniques described in this manuscript. Arguably a

635 better way of assessing common-Pb affected data is to first view it without common-Pb

636 correction on a Tera-Wasserburg (^{207}Pb/^{206}Pb vs. ^{238}U/^{206}Pb) diagram so that the true scatter

637 in the data can be seen as well as the trend in the data indicating the appropriate composition

638 to use for correction. Sometimes this trend is not visible within a cluster of data and the

639 analyst has no option but to assume a relevant composition based on other information.

640 However, particularly for non-zircon accessory phases, common-Pb compositional

641 constraints may be determined from U-Pb data with excess scatter, by initial plotting of data

642 that are not corrected for common-Pb, prior to the expansion of the uncertainties due to the

643 correction, and thus allowing the smaller data point uncertainties to better resolve these

644 components. Better resolution of the true scatter is important in defining whether the data do

645 indeed represent a single population, the fundamental assumption which must be adhered to

646 if the data are to be corrected. A common-Pb corrected age and uncertainty can then be more

647 appropriately defined in this way. Equivalent to a ^{207}Pb-based common-Pb correction, this

648 approach still ignores however, the potential for Pb-loss to also disturb the system, except in

649 that Pb-loss in addition to common-Pb would likely result in increased scatter of the data

650 population now better resolved with the uncorrected, more precise, data point uncertainties.

651 Anderson (2002) highlighted the limitations of ^{207}Pb and ^{208}Pb-based common-Pb corrections

652 in the presence of Pb-loss and illustrated an alternative approach, not requiring measurement

653 of ^{204}Pb (particularly for ICP-MS-based measurements), which accounted for non-zero age

654 Pb-loss within a data population. The potential for systematic errors after correction were

655 however noted at Pb-loss proportions greater than a few percent.

656 *2.3.5 Method work flow and data treatment*

657 Imaging is a critical first step in the LA-ICP-MS U-Th-Pb workflow. Cathodoluminescence

658 (CL), back-scattered electron (BSE), electron back-scattered diffraction (EBSD), elemental

659 maps and other sample characterization methods are important tools allowing precise

660 targeting of microbeam analyses and evidence-based interpretation of the data. Transmitted

661 light optical imagery is also useful for laser ablation work in conjunction with surface

662 images, to avoid common-Pb bearing sub-surface cracks and inclusions which might

663 otherwise be sampled during ablation. Ultimately the output data should be interpreted with

664 the image information in hand so that aberrant data points can be considered in the context of

665 their analysis position in the material, its complexity and the likelihood of encountering a

666 problem with depth.

667 Recent community-based efforts have sought to minimise systematic artefacts in laser

668 ablation U-Pb data to better understand their nature and determine appropriate data handling

669 routines and uncertainty propagation protocols. This LA-ICP-MS U-Th-Pb Network has

670 made recommendations for the appropriate handling, reporting and interpretation of LA-ICP-

671 MS U-Pb data (www.Plasmage.org;) which should result in improved standards (*sensu*

672 *stricto*) in this field of geochronology and lead ultimately to a reduction of the method

673 limiting uncertainty, perhaps to as little as 0.5% (2σ) for the Pb/U ratio. The method limiting

674 uncertainty reflects the community inter-laboratory comparison capability and requires

675 sources of systematic errors (*sensu stricto*) to be identified.

676 Although new data handling procedures have been recommended, until such time as these

677 become common-place amongst practitioners, variability of data treatment remains a

678 fundamental limitation in this field of geochronology. Until improved uncertainty assessment

679 is common practice, allowing better resolution and comprehension of data scatter,

680 improvements to analytical and instrumental set-up will not be achieved and inter-laboratory

681 comparison will remain at the ca. 2% (2σ) level.

682

683 **3. Limits on the interpretation of geochronologic dates**

684 *3.1 Correction for initial ^{230}Th and ^{231}Pa disequilibrium*

685 As a result of differing mineral-melt distribution coefficients (D) for the different elements

686 present within the ^{238}U and ^{235}U decay chains, crystallizing accessory minerals exclude or

687 enrich long-lived intermediate daughter products relative to their parent isotopes. For

688 geochronology, the two most relevant nuclides are the comparatively long-lived ^{230}Th (half-

689 life t½ = 75,584 a; Cheng et al., 2013) and ^{231}Pa (t½ = 32,760 a; Robert et al., 1969), which

690 for zircon are enriched or depleted, respectively, relative to secular equilibrium. Magmatic

691 processes do not fractionate ^{234}U (t½ = 245,620 years; Cheng et al., 2013) from its parent, but

692   recoil ejection and leaching can lead to ^{234}U loss and a resulting deficit in ^{206}Pb in radiation

693   damaged minerals (e.g., Romer, 2003; Cheng et al., 2013). Corrections for initial

694   disequilibrium require knowledge of the partitioning ratio between the U parent and a stable

695   proxy X for the intermediate daughter D_X/D_U (Schärer, 1984). For ^{230}Th, X = ^{232}Th is used,

696   with the Th/U of the melt estimated from the composition of whole-rocks, matrix glasses, or

697   melt inclusions (e.g., Crowley et al., 2007). If melt or fluid compositions are unknown,

698   experimentally or empirically derived D_X/D_U can be used (e.g., Blundy and Wood, 2003;

699   Rubatto and Hermann, 2007). No stable proxy is available for ^{231}Pa, the longest-lived

700   intermediate daughter in the ^{235}U decay chain. Lattice-strain partitioning models for the

701   incorporation of ^{231}Pa^{5+} into the zircon lattice predict high K_D values (Blundy and Wood,

702   2003), which is in agreement with $D_{Pa/U}$ = 3.8 ± 0.8 determined from direct analysis of ^{231}Pa

703   in late Pleistocene zircons and whole rocks (Schmitt, 2011). D_{Nb}/D_U or D_{Ta}/D_U zircon-melt

704   values theoretically permit extrapolation to unsupported ^{231}Pa at the time of zircon

705   crystallization, but this is confounded by uncertainties in the oxidation states of Pa and U

706   (Burnham and Berry, 2012). To completely circumvent the problem of initial intermediate

707   daughter disequilibrium, ^{208}Pb/^{232}Th ages can be determined. In that case, disequilibrium

708   effects are negligible due to the short half lives of the intermediate daughters (t½ <5.75 a;

709   Mays et al., 1962), e.g., applied to hydrothermal monazite (Janots et al., 2012).

710   For complete ^{230}Th exclusion from the zircon lattice, the resulting correction amounts to a

711   maximum of 110 ka on the ^{206}Pb/^{238}U date, using the ^{230}Th decay constant of Cheng et al.

712   (2013). This is non-negligible for time-scale work in young, astronomically-tuned

713   sedimentary sections, where the ^{230}Th disequilibrium correction may equal approximately

714   four to five precession cycles (Wotzlaw et al., 2014). When applying a disequilibrium

715   correction, initially distinct dates may converge (Fig. 1b). This example also illustrates that

716   the Th disequilibrium correction effect becomes larger than the total ^{206}Pb/^{238}U age

717   uncertainty for ID-TIMS dating of rocks <100 Ma, and the estimated 50% uncertainty on

718   D_{Th}/D_U becomes the dominant source of uncertainty for dates <10 Ma (Wotzlaw et al., 2014;

719   Fig. 1b). Zircon populations may show a large dispersal in Th/U (^{208}Pb/^{206}Pb) values that may

720   reflect variable Th/U of the magma from which they crystallized, or a variable D_X/D_U of

721   zircon at constant Th/U of the magma (see Rioux et al., 2012). For zircon, excess ^{207}Pb$_{rad}$ will

722   lead to erroneously old ^{207}Pb/^{235}U dates by up to 130 ka for D_{Pa}/D_U of 3.8 (Schmitt, 2011).

723   This means that any zircon <10 Ma will be measurably displaced to the right of concordia

724   due to uncorrected ^{231}Pa excess (Fig. 1b).

725

3.2 Protracted crystallization of igneous zircon

3.2.1 Insights from U-series studies

How fast does zircon crystallize in natural systems, and what are the limits on the dating accuracy if the sampling volume integrates over diachrononous crystal domains? U-series dating, mainly utilizing ^{230}Th/^{238}U disequilbrium, offers the highest absolute temporal resolution for recent crystals (e.g., Cooper and Kent, 2014). Moreover, SIMS depth profiles can interrogate crystal growth domains parallel to prism faces at sub-micron spatial resolution (Fig. 4). There is a growing data set for accessory minerals in youthful volcanic systems studied by U-series geochronology (e.g., Claiborne et al., 2010; Stelten et al., 2013), but for brevity we can only highlight results that bear directly on the interpretation of zircon ages. This is best done by focusing on a single study region, the Quaternary Taupo Volcanic Zone (TVZ) which embodies many characteristics of volcanic systems underlain by batholith-scale silicic magma bodies and which lends itself for a review because (1) its late Quaternary to recent age is ideal for high-temporal resolution U-series dating of zircon, (2) it preserves the products of high-frequency eruptions from multiple nested caldera systems, and (3) it has been studied by several research groups, thus providing an excellent opportunity to test different methodological approaches (Fig. 6).

Zircon populations from TVZ rhyolites and plutonic ejecta have been intensely studied by ID TIMS bulk and SIMS spot analysis, as well as SIMS studies using sectioned crystals and depth profiling of the outermost crystal margins (e.g., Charlier et al., 2003, 2005; Charlier and Wilson, 2010; Klemetti et al., 2011; Danišík et al., 2012; Shane et al., 2012; Storm et al., 2011, 2012; 2014), with results being largely complementary and mutually supportive. ID TIMS analysis of ~1 mg zircon separates comprising 100s of individual crystals for the Rotoiti eruption (~45 ka; Danišík et al., 2012) is in excellent agreement with the concentration-weighted SIMS average of multiple spots (~1 ng per spot; Charlier et al., 2003, 2005; Fig. 6). The stated precision of the TIMS age (approximately ±2 ka), however, is geologically meaningless in the light of protracted crystallization (>300 ka) revealed by SIMS spot analyses (e.g., Charlier et al., 2003).

Insert here Fig. 6

Detailed depth profiling studies of zircon in post-Rotoiti rhyolites erupted from Tarawera volcano (TVZ) have revealed that zircon crystal rims frequently predate the eruption (Storm

757 et al., 2011; 2012). Moreover, individual crystals record protracted crystallization, which can

758 be interrupted during recharge events due to increase of magma temperature and resorption of

759 zircon. Tarawera data also reveal that, despite some actual heterogeneity of rim ages, the

760 peak of the zircon rim age distribution progressively shifts towards younger age with

761 decreasing eruption age. Statistical comparison of zircon age probability density distribution

762 (PDD) curves further demonstrates that interior ages of the same population are

763 indistinguishable from the rim ages of the preceding eruption ("Storm's rule"; Fig. 6),

764 implying that pre-existing zircon in unerupted residual magma is a preferred nucleation site

765 for renewed crystallization. Trace element zoning within Tarawera zircons displays mostly

766 normal, retrograde (down-temperature) crystallization trends indicated by rimward

767 decreasing Zr/Hf and Ti (Fig. 7), but a significant (~30%) proportion of depth-profiled

768 zircons indicate crystallization following thermal and compositional reversals (i.e., rimward

769 increases of Zr/Hf and Ti; "recharge" in Fig. 7).

770 These observations collectively reveal that the zircon 'cargo' in volcanic rocks is sourced

771 from heterogeneous domains in the magma storage region where zircon crystallization

772 followed distinct thermal and compositional evolutionary paths. Moreover, the absence of

773 near-eruptive aged rims in some crystals indicates that zircon residence in the host magma is

774 often too short to directly record the conditions in the liquid-dominated, eruptible portion of a

775 magma reservoir. In favourable instances, plutonic clasts excavated during pyroclastic

776 eruptions provide additional insights into the compositional and thermal heterogeneity of

777 long-lived magma reservoirs. Where zircons in plutonic rocks formed synchronously to those

778 of their volcanic host, they have been interpreted as ripped up from highly crystalline mushes

779 (e.g., Charlier et al., 2003), whereas in other cases plutonic zircons predate those in co-

780 erupted volcanic rocks and may indicate an origin from older intrusive carapaces which acted

781 as barriers to the interaction of magma with country rock, but also are a potential source of

782 "old' zircons in subsequent eruptions (e.g., Shane et al., 2012).

783 The recognition of the complexity of zircon ages in young igneous rocks led to the

784 classification of Miller et al (2007) who distinguished an *autocrystic* population (youngest

785 grains that grew in equilibrium with the last magma batch in which they occur), and an

786 *antecrystic* population that is derived from earlier stages of magma evolution within the same

787 plumbing system and thus yielding older U-Pb dates (see example in Fig. 8), to be

788 distinguished from *xenocrystic* (zircon that is accidentally entrained into the magma) or

789 *inherited* zircon (derived from melting of a source rock). There are no clear boundaries

790 between these categories (Fig. 7). In particular, the difference between antecrystic and

791 autocrystic growth (according to the definition of Miller et al., 2007) merits some more

792 consideration: zircon is stable within a temperature window and a magma composition

793 characteristic for melt saturation for this mineral (Watson and Harrison, 1983; Boehnke et al.,

794 2013). This temperature may be repeatedly exceeded during recharge of a magmatic system

795 by incoming hot magma, leading to resorption and partial dissolution of previously

796 crystallizing zircon, followed by cooling down to temperatures of zircon saturation and

797 crystallization. Repeated cycling through the saturation temperature band commonly lasts for

798 a few 10's to 100's ka (e.g., Broderick 2013; Storm et al., 2011; 2012; 2014; Wotzlaw et al.,

799 2013), reflected by multiple peaks in PDD curves from multi-episodic zircon growth (Fig. 8a,

800 b). Because of the extended zircon crystallization in long-lived magma systems, zircon ages

801 cannot *a priori* be interpreted to record an instantaneous geologic event, with implications for

802 ID-TIMS dating discussed below.

803 *Insert here Fig 7*

804 *3.2.2 Scattered zircon U-Pb dates from high-precision ID-TIMS dating of igneous rocks*

805 The advent of the precisely calibrated EARTHTIME tracers, the chemical abrasion pre-

806 treatment and the use of linear and stable electron and photo multipliers for ion counting of

807 the minor Pb masses, has led to <0.1% precision on common-Pb corrected $^{206}Pb/^{238}U$ dates.

808 The low Pb_{rad}/Pb_{com} ratios, the uncertainty of the isotopic composition of the procedural blank

809 and the possibility of a common-Pb component in the zircon, renders the $^{207}Pb/^{235}U$ date

810 unreliable for Phanerozoic zircon (see Fig. 1b). The community focused on high-precision

811 dating of igneous rocks has therefore shifted away from the concordia-age concept (Ludwig,

812 2003) and is using instead a statistical approach on the $^{206}Pb/^{238}U$ date only. The data are

813 displayed as $^{206}Pb/^{238}U$ date-ranked distribution plots, and corresponding PDD curves (Fig 8).

814 High-precision ID-TIMS dates are obtained from a whole volume or a (mostly randomly

815 sampled) fragment of one single zircon grain, excluding only the decay-damaged zones that

816 have been mostly dissolved during chemical abrasion. The date therefore represents an

817 integrated history of crystallization over many growth zones. In the absence of radiogenic Pb

818 loss or inheritance, dispersion of ID-TIMS dates therefore always give a *minimum* period for

819 zircon crystallization in a given magmatic system. This approach implies removal of all

820 discordance within the zircon volume that survived the chemical abrasion treatment, an

821 assumption that cannot be proven in reality. Instead, perfect reproducibility within youngest

26

822 clusters of zircon dates, or coincidence with other chronometers such as U-Pb titanite, or

823 astrochronology (Wotzlaw et al., 2014) are used as arguments to support this assumption.

824   *Insert here Fig. 8*

825 High-precision ID-TIMS U-Pb dating is predominantly applied to questions related to magma

826 reservoir processes and for the reconstruction of the geological time scale, usually by dating

827 volcanic ash beds in sedimentary sections. In the case of a volcanic ash or flow the aim is to

828 date its eruption. The ^{206}Pb/^{238}U date of the youngest data cluster (assuming that it is not

829 biased by Pb loss) is commonly adopted as an approximation of the age of the last

830 crystallization; it then remains to quantify the time lapse Δt between the youngest zircon date

831 and final solidification or eruption. High-precision U-Pb dating of volcanic zircon in 4 to 12

832 Ma old ash beds from astrochronologically well-characterized upper Miocene sedimentary

833 successions demonstrates that in some cases Δt cannot be resolved because it is therefore

834 smaller than our analytical uncertainty of 4 to 12 ka; at the other extreme the Δt may reach a

835 few 100 ka (Wotzlaw et al., 2014). This means that for volcanic rocks >100 Ma, Δt is largely

836 negligible relative to analytical uncertainties.

837 The total dispersion of U-Th or ^{206}Pb/^{238}U dates in a zircon population characterizes the

838 temporal and spatial heterogeneity of magma bodies which may alternate between near-

839 solidus and partially re-molten states, and which are open to thermal and compositional

840 rejuvenation via magma recharge (e.g., Wotzlaw et al., 2013; Storm et al., 2014). Although

841 the dynamics of such magma systems are not entirely understood, it is conceivable that

842 liquids carrying suspended zircons (and other fine-grained minerals) separate from coarser-

843 grained solids, and that melt-zircon suspensions are transported towards higher crustal levels

844 due to buoyancy overpressure. Consequently, zircon age dispersion may not necessarily

845 record protracted zircon growth in a melt batch undergoing closed-system crystallization, but

846 may result from zircon crystallization in melts that were saturated at different times and that

847 were intermittently stored under conditions close to the magma solidus (Broderick, 2013;

848 Cooper and Kent, 2014). Based on thermal considerations, the time taken for effective

849 solidification at the level of final emplacement in the middle or upper crust is expected to be

850 one or two orders of magnitude shorter than the age dispersion of plutonic zircon populations.

851 The interpretation of zircon U-Pb ages in volcanic and plutonic systems may therefore be

852 very complex; zircon may be recycled from precursor mushes and crystallize at any time the

853 melt is zircon-saturated, be it during magma transfer through the crust, at emplacement, or

854 even during final cooling to the solidus and possibly hydrothermally under sub-solidus

855 conditions. A plutonic zircon date therefore marks simply a transient stage of "rheological

856 freezing" of a magma mush. The PDD curves derived from the distribution of $^{206}Pb/^{238}U$

857 zircon dates have been demonstrated to be related to magma volume and flux (Caricchi et al.,

858 2014) and may be used for quantitative modelling of these parameters.

859 A concern for representative sampling of a population is the number of grains analyzed. This

860 is generally more critical for CA-ID-TIMS dates where the time and effort to carry-out

861 individual analyses significantly exceeds that for SIMS or LA-ICP-MS, especially in cases of

862 obviously complex zircon populations. Experience shows that 10-20 analyses are needed to

863 interpret a complex population with sufficient confidence; if applied as a chronostratigraphic

864 tool to a sedimentary succession, a high sample density is required in addition, to recognize

865 complex magmatic behaviour of the U-Pb system in zircon (Guex et al., 2012; Wotzlaw et

866 al., 2013, 2014).

867

868 *3.3 Scattered vs. clustered U-Th-Pb dates: data point precision and uncertainties on average*

869 *ages*

870 Irrespective of the analytical method, the uncertainty in individual isotopic measurements or

871 data points determines ones ability to resolve scatter within a data set and to discriminate one

872 data population from another. Most samples of volcanic and plutonic rocks contain zircons

873 with a range of dates that may or may not be resolvable, depending on the uncertainty of the

874 technique used (see, as an example, the history of U-Pb dating of the Fish Canyon Tuff;

875 Schmitz and Bowring, 2001; Bachmann et al., 2007, Wotzlaw et al., 2013). In order to

876 evaluate whether the scatter may reflect solely analytical uncertainty, in which case it would

877 be appropriate to calculate a weighted mean $^{206}Pb/^{238}U$ age, or whether it contains a

878 component of excess scatter, the mean square weighted deviation (MSWD) is evaluated. For

879 a large number of analyses, a MSWD ≈ 1 (with the exact range of permissible values

880 calculated from the number of analyses N averaged in the calculation; Wendt and Carl, 1991;

881 Mahon, 1996) indicates scatter from analytical uncertainty only and/or has scatter

882 unresolvable at the level of the assigned data point uncertainty (Kalsbeek, 1992). By

883 calculating a weighted mean age we imply that all zircons have crystallized simultaneously

884 within analytical resolution, or that any age difference remains unresolved within uncertainty.

885 Zircon populations with excess scatter will yield unacceptably high MSWD values at a given

886 N and have to be interpreted in terms of real age dispersion (or open system behaviour) after
887 any analytical bias has been ruled out. It is important to emphasize that even for zircon
888 populations with no analytically resolvable scatter (i.e., MSWD = 1), it would be fallacious to
889 interpret the limits of the uncertainty-weighted average as an indication for the actual
890 duration of zircon crystallization. It is the analytical uncertainty of the individual
891 measurements which dictates the capability to define a single population, and one may not *a*
892 *priori* assume homogeneity in the population below this limit.

893 In addition it should be noted that a single population of data validated by MSWD statistics
894 does not preclude a systematic error (i.e. bias) being present within the dataset. Sample
895 results using a relative method cannot therefore be any more accurate (i.e. including
896 precision) than the level to which the relevant reference materials are defined. Therefore, one
897 of the fundamental limiting uncertainties for SIMS and LA-ICP-MS is the uncertainty in the
898 composition of the reference zircon being used (Table 2). Systematic uncertainties (e.g., from
899 tracer calibration in the case of ID-TIMS, or from decay constant determination) do affect
900 data accuracy despite apparent high precision, and need to be propagated into final
901 uncertainties when comparing between data from different techniques or to data from other
902 chronometers.

903

904 *3.4 Efficiency of chemical abrasion in ID-TIMS, SIMS, and LA-ICP-MS*

905 The approach of focusing on the youngest sub-population of zircon grains requires that any
906 trace of post-crystallization radiogenic Pb loss has been removed during the chemical
907 abrasion treatment (Mattinson, 2005). There remains, however, the suspicion that a residual
908 Pb loss component can influence the U-Pb date of the youngest zircons in a population,
909 predominantly in ash beds that suffered post-depositional fluxing by aqueous solutions and
910 volatiles. Whether a given analysis is biased by residual Pb loss or not is often a subjective
911 decision. Failure to report such data in the data table of a scientific publication is poor
912 practice that prevents eventual re-assessment of previously erroneously interpreted data.

913 Since chemical abrasion is a purely empirical procedure, it may be desirable to develop
914 proxies in the future to detect minor traces of Pb loss. In addition, we need to be aware that
915 chemical abrasion is preferentially removing the zones richest in U, thus biasing the U-Pb
916 data towards, marginal or more internal, low-U growth zones (Fig. 7). How can "pathologic"
917 behavior of the U-Pb system (e.g., Pb-loss, inheritance, and to minor extent initial

918   disequilibrium) be distinguished from true variations in crystallization age, and how much

919   bias do we actually introduce through chemical abrasion? The high degree of reproducibility

920   of chemically-abraded zircon dates in inter-laboratory cross-calibrations on natural zircon

921   populations suggests that we can be rather optimistic in this respect, if we respect the limiting

922   parameters and analyse a sufficient number of zircon crystals. These studies, however,

923   employ mostly high-quality materials that have been proposed as international reference

924   materials, which more easily reproduce their high-precision age.

925   A number of studies have now also identified the potential utility of thermal annealing or

926   chemical abrasion for SIMS (Kryza et al., 2012) and LA-ICP-MS (Allen and Campbell,

927   2012; Marillo-Sialer et al., 2014; Crowley et al., 2014; von Quadt et al., 2014). Most studies

928   demonstrate reduced ablation rates for thermally annealed or chemically abraded material

929   when compared to ablation rates in untreated materials and improved concordance (reduced

930   Pb-loss/common-Pb effects) of final results. Allen and Campbell (2012) cite the annealing of

931   alpha recoil tracks and structural harmonization as the mechanism for a reduced ablation rate

932   and improved validation to better than 1% accuracy, whilst Marillo-Sialer et al. (2014)

933   indicate that the relative deviations between validation materials remain after annealing

934   although ablation rates are reduced. Crowley et al. (2014) recognise reduced ablation rates

935   even for Archaean zircons despite the mineral structure becoming more porous after

936   widespread partial dissolution after chemical abrasion and von Quadt et al. (2014) also

937   illustrate reduced Pb-loss effects, greater geological accuracy of the results and improved

938   precision due to a reduction of scatter within the chemically abraded data populations.

939   However, since both SIMS and LA-ICP-MS techniques are described as requiring

940   compositional and structural homogeneity between sample and reference materials to obtain

941   appropriate calibrations, the indiscriminate application of chemical abrasion preparation

942   procedures for samples could lead to increased variability in both parameters relative to the

943   reference materials. Unless extensive unleached (low U) portions of the sample crystal are

944   preserved, the dissolution part of the chemical abrasion procedure may result in extensive

945   structural differences between samples and reference materials, exacerbating the variability

946   of ablation rates and indeed increasing it significantly. Clearly then chemical abrasion and/or

947   thermal annealing has a significant role to play in improving the method uncertainty limit and

948   overall accuracy of SIMS and LA-ICP-MS U-Pb dates, but greater clarification of the effects

949   of this approach are still required not least to ascertain the effect for complex zircons with

950   multiple age domains which might be removed by the abrasion process. The value of high

951 spatial resolution techniques is in illustrating the presence of such previously unrecognised

952 domains whilst attempting to date them. Their removal prior to their recognition could be

953 considered a backward step.

954 It should be noted that for zircon dated by high spatial resolution techniques from material

955 that is not pre-treated by chemical abrasion techniques it is not appropriate to apply the

956 common strategy used by CA-ID-TIMS specialists to adopt the youngest analysis as a proxy

957 for the last crystallization event in a magma, because such a date is potentially biased by Pb

958 loss. In the same way, single laser ablation or SIMS analyses from detrital zircon spectra

959 should not be used to interpret the maximum depositional age of sediments. This is best

960 estimated from the average of multiple young dates overlapping within analytical uncertainty

961 (Dickinson and Gehrels 2009; see recommendations on www.Plasmage.org) and regardless

962 of whether CA pre-treatment was applied or not.

963

964 *3.5 Reference materials*

965 SIMS and LA-ICP-MS U-Th-Pb dating are comparative methods dependent on reference

966 materials for determining RSF values for inter-element ratio corrections. They therefore

967 require suitable natural or artificial reference materials, of similar elemental concentration

968 and structural state to the unknowns, homogenous in age and ideally also Th/U and trace

969 elements. There are currently very few well-characterized reference materials available

970 (Table 2) and many with insufficient ID-TIMS age control. This limitation means that a

971 SIMS or LA-ICP-MS date can only be as good as the homogeneity of the reference materials,

972 the accuracy and precision to which such material is known, as well as the stability of the

973 system during analysis (see section 3.3; Table 2). Some materials are well defined at ca. 0.1%

974 ([x] uncertainty; 2σ) of their $^{206}Pb/^{238}U$ age (e.g., Plešovice, Sláma et al., 2008, or AUSZ2,

975 Kennedy et al., 2014). For other materials, e.g., the Mud Tank zircon (Black and Gulson,

976 1978) and many of the monazite, rutile and titanite reference materials, this can be as bad as

977 3-4% (2σ, $^{206}Pb/^{238}U$ age). Concerning homogeneity, some of these "candidate reference

978 materials" are far from being ideal, especially for non-zircon phases, but are simply all that is

979 available. There is also a dearth of well-characterized Quaternary reference materials, where

980 analytical challenges are highest because of low signals, crystallization age heterogeneity and

981 initial isotopic disequilibrium.

982 The Plešovice zircon was demonstrated to perhaps have some age and/or matrix variation

983 impacting on SIMS dates and likely also consistency of laser ablation results (Sláma et al.,

984 2008). U variations within Plesovice crystals are as high as 465-3084 ppm, resulting in

985 metamict areas with increased ablation rate and therefore downhole fractionation. The GJ-1

986 zircon appears very homogeneous for age within one crystal but different crystals are claimed

987 to have slightly different ID-TIMS reference U-Pb ages (Jackson et al., 2004; Schaltegger et

988 al., unpubl., in Boekhout et al., 2012).

989 It should be ensured that relevant reference values are used in reference to the relevant

990 sample value. Comparing the Pb/U result for a material to its expected concordia age for

991 example, is invalid and gives a false impression of accuracy, positively or negatively. Since

992 few of the known 'candidate reference materials' for in situ U-Th-Pb geochronology, are

993 concordant within the precision limits of the reference data (e.g. GJ-1, 91500), comparison of

994 the correct reference ratio with the equivalent sample ratio is imperative. This is particularly

995 important for non-zircon accessory phases which are increasingly the focus of research.

996 Apatite (Chew et al., 2011; Thomson et al., 2012), rutile (Kooijman et al., 2010; Zack et al.,

997 2011; Schmitt and Zack, 2012), titanite (Storey et al., 2006) and monazite (Harrison et al.,

998 1995; Košler et al., 2001; Hietpas et al., 2010) all incorporate initial Pb to greater or lesser

999 extents and commonly contain excess ^{206}Pb due to incorporation of excess ^{230}Th during

1000 crystallization. Reference values reflecting the exact composition of the material sampled are

1001 therefore required.

1002 Ultimately, at the smallest scale, no reference material will be compositionally or structurally

1003 matrix-matched to an unknown. Recent individual and community efforts have attempted to

1004 compile a list of available reference materials for laser ablation U-Th-Pb geochronology. The

1005 Arizona LaserChron Centre (https://sites.google.com/a/laserchron.org/laserchron/) and the

1006 LA-ICP-MS U-Th-Pb Network (www.plasmage.org) detail lists of materials, their

1007 availability and origin.

1008

1009 *3.6 Zircon U-Pb precision in comparison with other accessory minerals*

1010 As shown above, minerals other than zircon - with the exception of monazite, xenotime and

1011 baddeleyite - have distinctly lower Pb_{rad}/Pb_{com} ratios and therefore cannot yield U-Pb dates at

1012 the same level of precision as zircon (see, e.g., Schoene et al., 2012). Correct uncertainty

1013 propagation of the isotope composition used for Pb_{com} correction is essential to obtain an

1014   accurate ^{206}Pb/^{238}U age with correct associated uncertainty from these minerals. An

1015   optimized approach is to measure Pb$_{com}$ in low-U phases such as feldspars and assume

1016   equilibrium with crystallizing zircon, instead of blindly using a model isotope composition

1017   from the crustal growth model of Stacey and Kramers (1975), evidently not possible for

1018   detrital minerals. For assessing the uncertainty of the Pb$_{com}$ isotope composition, we can

1019   propagate the analytical uncertainty from the feldspar analyses, or model uncertainty limits

1020   taking the most extreme Pb$_{com}$ isotope compositions found in the studied rocks. The

1021   application of the 3D isochron approach may evidence non-common, slightly radiogenic

1022   initial Pb isotope compositions, but is biased by the fact that, e.g., titanite crystallizes over a

1023   significant time span and therefore different single grains are not strictly coeval (Schoene et

1024   al., 2012).

1025   Additional complication is presented in the case of baddeleyite which often shows effects of

1026   post-crystallization lead loss. Chemical abrasion or leaching treatment prior to analysis

1027   proved to be inefficient and leads to analytical artifacts (Rioux et al., 2010); the accuracy of

1028   baddeleyite and zircon data is therefore often not entirely equivalent.

1029   High-precision monazite dating is hampered by initial ^{230}Th disequilibrium leading to

1030   unsupported radiogenic ^{206}Pb, which cannot be corrected in a metamorphic environment

1031   since the Th/U of the crystallizing medium is not known. This obstacle may be overcome by

1032   using the ^{207}Pb/^{235}U date at marginally lower precision, or to use the ^{208}Pb/^{232}Th isotopic

1033   systems instead, especially for SIMS and LA-ICP-MS.

1034

1035

1036   **4. Improving the interpretation of geochronologic data**

1037   *4.1 Imaging and texturally controlled sampling*

1038   Cathodoluminescence (CL) imaging for zircon, back-scattered electron (BSE) imaging and

1039   electron probe elemental maps (for monazite and other accessory phases with complex

1040   chemical zoning) are essential aids for guiding selection of analysis locations for high spatial

1041   resolution dating studies (and increasingly for selecting crystals or crystal domains for high-

1042   precision ID-TIMS analysis) and help enable robust interpretations of U-Th-Pb data. Without

1043   knowledge of what is being analysed, a result, however precise, is less meaningful or even

1044   non-interpretable. Increasingly, techniques such as electron back-scattered diffraction

1045   (EBSD; e.g., Moser et al., 2009; Fig. 9a), SIMS ion imaging (e.g., Kusiak et al., 2013),charge

1046 contrast imaging (CCI; Watt et al., 2000; Fig. 9b), Raman spectroscopy (e.g., White and

1047 Ireland, 2012), and transmission electron microscopy (TEM; e.g., Dobrzhinetskaya et al.,

1048 2014) are also coming to the fore, demonstrating the relationship between structural

1049 coherency of the material, crystal orientation, inclusions, contamination, and the significance

1050 of geochronological data.

1051 The combination of imaging methods and U-Th-Pb age data, in providing compositional and

1052 structural variation information related to age, provides for much more powerful

1053 interpretations and better quality control of data. When consulted during data interpretation,

1054 imaging can help distinguish between isotopic results that are biased by lead loss and

1055 inheritance (or antecrystic zircon growth). However, although CL imaging is most prevalent,

1056 distinct boundaries between CL zones do not necessarily correlate with detectable age

1057 differences within a grain, locations of disturbance, or thermochemical boundaries.

1058 Conversely, zircon crystallization hiatuses have been documented by U-Th dating in young

1059 magmatic systems where CL images show no obvious discontinuities (Storm et al., 2011).

1060 *Insert here Fig. 9*

1061 While CL often gives a qualitative idea about the degree of complexity of the growth

1062 structures, other imaging techniques can reveal more reliable insights into the crystal

1063 structure (e.g., EBSD) and zonation (e.g., CCI). Moreover, repeated recharge of a magmatic

1064 system with increased temperature may lead to periods of dissolution (resorption) followed

1065 by growth again when saturation conditions are achieved. This leads to very complex internal

1066 textures of magmatic zircon formed over timespans that may not be resolved by high-

1067 precision ID-TIMS dating and whose detection may require ultrahigh-spatial resolution

1068 techniques such as depth profiling (e.g., Fig. 7).

1069

1070 *4.2 In-situ and ultra-high spatial resolution analysis*

1071 High-spatial resolution techniques can directly target crystals in polished petrographic

1072 sections (*in situ* analysis *sensu stricto*). In-situ dating offers several advantages: (1)

1073 preservation of textures and context (e.g., linking metamorphic textures and parageneses to

1074 accessory mineral growth; Foster et al., 2004; Möller et al., 2003; Catlos et al., 2002); (2)

1075 accessibility of micro-crystals, inclusions, or epitaxial overgrowths which are otherwise

1076 difficult or impossible to separate (e.g., micro-baddeleyite; Schmitt et al., 2010; micro-zircon;

1077 Ault et al., 2012; diagenetic zircon overgrowths; Rasmussen, 2005); (3) avoiding

contamination (Hellebrand et al., 2007) and (4) the possibility to target armoured crystals which may be protected from later fluid events that mobilized Pb in radiation damaged crystals (e.g., Ault et al., 2012; Fig. 10). To facilitate targeting and minimize sample changes, pieces from the sections are cut or drilled out, and mounted together with pre-polished reference grains for SIMS, or for laser ablation multiple thin sections are simply loaded into the larger sample chamber. If micro-crystals are analyzed, laser or ion beam overlap onto adjacent minerals with high common-Pb potentially reduces radiogenic yields, but this can be mitigated through a more constrained sampling beam, i.e., use of a smaller laser spot size or, in the case of CAMECA ims instruments, narrowing secondary beam apertures ("field" and "contrast" apertures; Figs. 4 and 10) to preferentially select ions from the interior of the crater and ions with a near-perpendicular take-off angle, respectively.

Of course one disadvantage to *in situ* analysis of materials in thin section is that they cannot be treated using chemical abrasion to reduce Pb-loss. The potential for Pb-loss to affect the data has therefore to be taken into consideration during the interpretation of *in situ* data. However, the added benefit of textural context may outweigh the potential for complications from Pb-loss in the case of zircon data and for some accessory mineral data (e.g. monazites), data interpretation is virtually useless without petrographic context and Pb-loss problems in monazites are considered to be minimal.

Insert here Fig. 10

Depth profiling of zircon by SIMS (e.g., Fig. 11; Vorhies et al., 2013) or single-shot LA-ICP-MS (Cottle et al., 2009) is a viable technique revealing age variations on the 100 nm scale. Addition of tiny zircon layers during metamorphism was investigated by Vorhies et al. (2013) on detrital zircons from the Barrovian Complex (Scotland; see Fig. 11) where SIMS depth profiles of grain faces revealed thin (often <1 μm) zircon rims with low Th/U in greenschist to K-feldspar-sillimanite grade rocks. Only zircon from the highest grade rocks produced rims and marginal domains >10 μm in thickness that could be detected by conventional spot analysis on sectioned crystals. However, as discussed in Cottle et al. (2009), surface analysis of zircons using depth profiling methods to reveal ages of the crystal rim are prone to Pb loss and common-Pb effects. For young material (<100 Ma), the Pb-loss trajectory is tangential to the concordia curve and indistinguishable from concordance at the uncertainties of microprobe data. These data therefore need considered interpretation to take such factors into account.

Insert here Fig. 11

1111

1112   *4.3. Combining data sets from different techniques and analytical approaches - Harnessing*

1113   *the full potential of high spatial resolution and high-precision methods*

1114   Ultimately, one of the factors limiting the accuracy of U-Pb data interpretation, is the quality

1115   and nature of the data themselves. Our ability to discriminate between two similarly aged

1116   materials or data points within data sets, is greatly increased by combining these data with

1117   other information. The complexity of accessory minerals at sub-grain to population level

1118   precludes any automation in date interpretation, but requires careful evaluation of additional

1119   and independent, chemical and physical information from the analysed material, to arrive at

1120   an accurate interpretation. Structural and chemical image analysis, or trace element and

1121   isotope chemical composition, add additional information upon which to base an assessment

1122   of single population status or exclude data points from the calculation of an average. The

1123   best, most robust dates will have proven their single population status through independent

1124   information (e.g., co-registered trace element or isotopic analyses) rather than 'blindly'

1125   assuming it based only on the MSWD statistic of the U-Pb data. In addition, high-precision

1126   and/or high-spatial resolution geochronology can now 'map out' changing processes such as

1127   magmatic differentiation and the crystallization history of a complexly zoned zircon and

1128   allow interpretation of the rate of chemical and geological evolution.

1129   Trace element information can help to characterize the crystallization history of zircon in

1130   different evolving melt batches over periods of 10's to 100's ka (Claiborne et al., 2010;

1131   Schoene et al., 2012). We may use specific trace element characteristics, such as depletions

1132   in Th/U or increases in Yb/Gd, produced by fractionation through co-precipitating accessory

1133   phases (e.g., monazite or titanite), which are characteristic of equilibrium with the last melt.

1134   When zircon crystallizes in a magma containing a certain percentage of crystals (a crystal

1135   mush), the trace elements of the U-Pb dated zircon can be used to model the chemical

1136   evolution of melts over time, employing published zircon - melt partition coefficients

1137   (Rubatto and Hermann, 2007; Blundy and Wood, 2003). The melt signal, in turn, can

1138   subsequently be used to infer the fractionation path of the co-precipitating paragenesis during

1139   solidification, and infer the proportion of crystallized material in the magma at any time.

1140   Petrological models for melt evolution and emplacement sequence can therefore be tested

1141   quantitatively. Timescales of crystallisation and fractionation have been established for the

1142   evolution of the Fish Canyon Tuff magma by using this approach, demonstrating that the

1143   assemblage containing 0.4 vol-% titanite formed over ~ 250 ka, starting at ~28.6 Ma when

zircon saturation was reached in a magma with 40% crystals, reaching a near-solidus state at 28.4 Ma with 76% crystals, followed by thermal rejuvenation and remelting over 170 ka, and ultimately eruption at 28.2 Ma when the magma contained ~45% crystals (Wotzlaw et al., 2013; Fig. 12). The curved trend in Fig. 12 is therefore not equivalent to a liquid line of descent, but consists of thermal prograde and retrograde paths acquired during the history of the Fish Canyon Tuff magma system. Zircon thus reflects repeated re-dissolution and re-precipitation during thermal cycling of a periodically recharged magmatic system, with most of the grains recording an age of 28.4 Ma, i.e., 200 ka before eruption. The isotopic and elemental budget of a whole zircon grain is dominated by the outer growth zones because of volume considerations; the whole grain isotopic and trace element information can therefore be considered to closely approximate equilibrium with the last melt batches. Recharge can also produce a late generation of zircon which can have the opposite characteristics to earlier zircon crystallized from more evolved melts (e.g., Rivera et al., 2013).

Insert here Fig. 12

Geochronological studies should evolve to increasingly include the collection of trace element and isotope (Hf and O) data in addition to U-(Th-)Pb. This can be achieved in a number of ways. ID-TIMS analysis of whole zircons or fragments historically discarded the material separated during ion chromatographic purification which contains many petrologically useful minor and trace elements. These solutions are now commonly retained for Hf isotope (Davis et al., 2005) and trace element (Schoene et al., 2012) analysis, the latter reference coining the term 'TIMS-TEA'. This approach benefits from the fact that all data are representative of the same dissolved volume and goes some way to off-setting the problems of 'bulk' sampling for TIMS analysis when considering spatial variation within the sample material. Alternatively, high spatial resolution methods can be used to provide all of this information (albeit at lower precision) with the added benefit of spatially controlled sampling. Laser ablation-ICP-MS and SIMS techniques are complimentary in this approach and should therefore be used depending on the number of information sets required, the available volume of material and/or the volume within which analyses need to be constrained. To this end, O and Hf isotopes provide important crustal generation indicators and are determined by SIMS and LA-ICP-MS respectively. Either method can also determine the U-Pb and trace element data, so spatial resolution considerations should determine which technique is used. In order to maximize the amount of information obtained from a zircon whilst consuming the minimum amount of material, O isotope, U-Pb and trace element data

1177 should preferentially be gathered by SIMS with Hf isotopes afterwards by LA-ICP-MS. With

1178 a moderate sacrifice in volume, the U-Pb and trace element data can also be determined by

1179 LA-ICP-MS. Increasingly, a 'split-stream' approach (Spencer et al., 2013, Kylander-Clark et

1180 al., 2013, Cottle et al., 2012) is being preferred for LA-ICP-MS analyses where the sample

1181 stream from one laser is split between two mass spectrometers to determine the Hf isotopes

1182 (or Nd isotopes in monazite, Goudie et al., 2014) and U-Pb or trace elements on exactly the

1183 same ablated volume. Used carefully this can help to reduce the total volume utilized whilst

1184 obtaining the maximum amount of information from a limited amount of sample material.

1185 However, the comparison of time-resolved data between the two mass spectrometers can be

1186 complicated by slight differences in instrumental set-up (e.g. tube lengths, connections,

1187 differential volumes and integration times) sometimes making the interpretation of data

1188 within an analysis difficult. In addition, if the total volume ablated for the split stream

1189 approach is greater than that required for the acquisition of one of the information sets alone,

1190 the benefit of the approach is lessened.

1191 For isotopically uniform or structurally simple crystals, the ultimate approach is to determine

1192 the required elemental and isotopic data set by high-spatial resolution methods whilst

1193 subsequently analyzing the smallest possible portion of the crystal to obtain a high-precision

1194 U-Pb age (Rivera et al., 2014), preferably then comparing the Hf and trace elements from the

1195 wash with those data determined by high-spatial resolution (Broderick, 2013). By combining

1196 data sets from different techniques and analytical approaches, well-constrained, accurate

1197 geochronological interpretations can be made and geological interpretations greatly improved

1198 and substantiated.

1199 Although zircon provides the most precise U-Pb data (see section 3.6) its extremely sluggish

1200 diffusion precludes the extraction of meaningful cooling rates and insights into lower

1201 temperature processes, unless (U-Th)/He data are acquired for these purposes. However, the

1202 combination of zircon with chronometers of lower retentivity (e.g., apatite, rutile, or titanite)

1203 to define P-T-t paths and fluid histories (e.g., Parrish et al., 2006; Rubatto, 2002) is a

1204 powerful tool to more completely understand tectonic and hydrothermal histories.

1205

1206 *5. Summary and forward look*

1207 We have undoubtedly entered a new era for U-Th-Pb geochronology. Unprecedented levels

1208 of precision, spatial resolution, flexibility of approach and range of application are now

1209 possible at increasingly higher analytical efficiency, and access to this capability for

1210 geoscientists is ever increasing. It might be asked "What is the best method or approach for

1211 U-Th-Pb dating?" Increasingly, the answer is "the one with appropriate precision and spatial

1212 resolution to answer your scientific questions appropriately, that can be demonstrated to work

1213 by validation and can be best tied most directly to other information sets". Most likely this

1214 will mean using capabilities not available in your laboratory! Whichever single or combined

1215 approach is selected, TIMS, SIMS or LA-ICP-MS, it is important to comprehend the

1216 limitations of the techniques, not to over-interpret the data and to quantify the uncertainties

1217 correctly. The relevant questions must be asked at the beginning of a project and the

1218 analytical techniques and approaches chosen with consideration. For timescale research,

1219 highest precision and accuracy is required; this can only be provided by CA-ID-TIMS using

1220 EARTHTIME calibrated isotopic tracers and careful statistical data treatment (Schoene et al.,

1221 2006, 2013; Bowring et al., 2005; Bowring et al., 2011; McLean et al., 2011b). CA-ID-TIMS

1222 is also required to resolve comparatively ancient (>0.5 Ma) magmatic emplacement pulses

1223 (Schoene et al., 2012; Broderick, 2013) but for late Pleistocene to recent systems (<0.3 Ma)

1224 only U-Th SIMS (e.g., Claiborne et al., 2011; Schmitt, 2011), and more recently LA-ICP-MS

1225 (Bernal et al., 2014) analysis can provide the necessary temporal and spatial resolution. For

1226 the lowest volume analysis of the most precious materials (e.g. lunar accessory minerals;

1227 Grange et al., 2013; Rasmussen et al., 2011) and minerals with fine scale growth domains,

1228 SIMS is the method of choice, as well as for highest-resolution isotopic mapping and depth

1229 profiling. For the efficient accumulation of large data sets at a ± 1-2% level of uncertainty

1230 and deeper depth profiling, LA-ICP-MS U-Pb dating is superior, and has to a great extent

1231 become the method of choice for detrital provenance and reconnaissance studies. There is

1232 still a large gap in the study of complex, ancient zircons (as, e.g., in Phanerozoic

1233 metamorphic complexes), where we need high spatial resolution for dating, analysis of other

1234 isotope systems and trace elements, but also would need high precision to decipher the

1235 sequence of metamorphic reactions.

1236 In this new era we should discourage acceptance and publication of studies employing

1237 analytical techniques with uncertainties greater than the duration of processes required to be

1238 resolved. Averaging large numbers of low-precision analyses has repeatedly been

1239 demonstrated to produce rather precise but inaccurate average age information. Equally, in

1240 some circumstances, the true duration of events might not be determined (due to bulk

1241   averaging), until lower precision, higher spatial resolution methods have been employed. The

1242   right tool for the job in hand must therefore be employed.

1243   The geochronology community has taken great strides and expended much effort to

1244   understand its data quality better and how it should best be represented, as for instance in the

1245   frame of the EARTHTIME and LA-ICP-MS U-Th-Pb Network efforts. It is no longer

1246   acceptable to submit manuscripts that do not characterize the different uncertainty levels,

1247   differentiate random and systematic uncertainties, report acquisition and data handling

1248   parameters appropriately or do not give any proof of accuracy and laboratory reproducibility

1249   by presenting results for internationally validated reference materials. Reviewers should insist

1250   on these information sets and editors should refuse to accept manuscripts for review or

1251   publication without them. The reason for this is simple: interpretations and models - often

1252   considered to be the most important part of a manuscript - may be subject to change of

1253   paradigms, whilst high-quality data remain. Any geochronologic study can only persist, if

1254   data are established using state of the art technology, are supported by the most

1255   comprehensive sample characterization possible, and are well documented.

1256

1264

1265   **References:**

1266   Allen, C.M., Campbell, I.H., 2012. Identification and elimination of a matrix-induced systematic error in LA–

1267   ICP–MS 206Pb/238U dating of zircon. Chem. Geol. 332–333, 157-165.

1268   Amelin, Y., Davies, D.W., Davies, W.J., 2005. Decoupled fractionation of even- and odd-mass isotopes of Pb in

1269   TIMS. Geochim. Cosmochim. Acta 69, A215

1270   Anderson, T. 2002. Correction of common-Pb in U-Pb analyses that do not report ^{204}Pb. Chem. Geol. 192, 59-

1271   79.

1272   Ault, A.K., Flowers, R.M., Mahan, K.H., 2012. Quartz shielding of sub-10 μm zircons from radiation damage-

1273   enhanced Pb loss: An example from a metamorphosed mafic dike, northwestern Wyoming craton. Earth

1274   Planet. Sci. Lett. 339-340, 57-66.

1275   Bachmann, O., Oberli, F., Dungan, M., Meier, M., Mundil, R., Fischer, H., 2007. 40Ar/39Ar and U–Pb dating

1276   of the Fish Canyon magmatic system, San Juan Volcanic field, Colorado: evidence for an extended

1277   crystallization history. Chem. Geol. 236, 134–166.

1278   Baldwin, S.L., Ireland, T.R., 1995. A tale of two eras: Pliocene-Pleistocene unroofing of Cenozoic and late

1279   Archean zircons from active metamorphic core complexes, Solomon Sea, Papua New Guinea. Geology 23,

1280   1023-1026.

1281   Bernal, J.P., Solari, L.A., Gómez-Tuena, A., Ortega-Obregón, C., Mori, L., Vega-González, M., Espinosa-

1282   Arbeláez, D.G., 2014. In-situ ^{230}Th/U dating of Quaternary zircons using LA-MC ICP MS. Quat. Geochron.

1283   23, 46-55.

1284   Black, L.P., Gulson, B.L., 1978. The age of the Mud Tank carbonatite, Strangeways Range, Northern Territory.

1285   BMR J. Austr. Geol. Geophys. 3, 227–232.

1286   Black, L.P., Kamo, S.L., Allen, C.M., Aleinikoff, J.N., Davis, D.W., Korsch, R.J., Foudoulis, C., 2003.

1287   TEMORA 1: a new zircon standard for Phanerozoic U–Pb geochronology. Chem. Geol. 200, 155–170.

1288   Black, L.P., Kamo, S.L., Allen, C.M., Davis, D.W., Aleinikoff, J.N., Valley, J.W., Mundil, R., Campbell, I.H.,

1289   Korsch, R.J., Williams, I.S:, Foudoulis C., 2004. Improved ^{206}Pb/^{238}U microprobe geochronology by the

1290   monitoring of a trace-element-related matrix effect; SHRIMP, ID–TIMS, ELA–ICP–MS and oxygen isotope

1291   documentation for a series of zircon standards. Chem. Geol. 205, 115–140.

1292   Blundy, J., Wood, B., 2003. Partitioning of trace elements between crystals and melts. Earth Planet. Sci. Lett.

1293   210, 383–397.

1294   Boehnke, P., Harrison, T.M., 2014. A meta-analysis of geochronologically relevant half-lives: what's the best

1295   decay constant?. Int. Geol..Rev. 56, 905-914.

1296   Boehnke, P., Watson, E.B., Trail, D., Harrison, T. M., Schmitt, A.K. (2013). Chem. Geol. 351, 324–334.

1297   Boekhout, F., Spikings, R., Sempere, T., Chiaradia, M., Ulianov, A., Schaltegger, U., 2012. Mesozoic arc

1298   magmatism along the southern Peruvian margin during Gondwana breakup and dispersal. Lithos 146-147,

1299   48–64.

1300   Bosse, V., Boulvais, P., Gautier, P., Tiepolo, M., Ruffet, G., Devidal, J. L., Cherneva, Z., Gerjikov, I., Paquette,

1301   J. L., 2009. Fluid-induced disturbance of the monazite Th–Pb chronometer: in situ dating and element

1302   mapping in pegmatites from the Rhodope (Greece, Bulgaria). Chem. Geol. 261, 286-302.

1303   Bowring, S.A., Erwin, D., Parrish, R.R., Renne, P., 2005. EARTHTIME: A community-based effort towards

1304   high-precision calibration of earth history. Geochim. Cosmochim. Acta, 69, A316–A316.

1305   Bowring, J.F., Horstwood, M.S.A., Gehrels, G., 2013. Resolving bias in laser ablation geochronology. Eos, Vol.

1306   94, No. 24.

1307   Bowring, J.F., Mclean, N.M., Bowring, S.A., 2011. Engineering cyber infrastructure for U-Pb geochronology:

1308   Tripoli and U-Pb_Redux. Geochem. Geophys. Geosyst. 12, Q0AA19. doi:10.1029/2010GC003479.

1309   Broderick C., 2013. Timescales and petrological processes during incremental pluton assembly: a case study

1310   from the Val Fredda Complex, Adamello Batholith, N. Italy. Unpubl. Thesis no. 4612 Univ. de Genève,

1311   169pp.

1312   Burnham, A.D., Berry, A.J., 2012. An experimental study of trace element partitioning between zircon and melt
1313   as a function of oxygen fugacity. Geochimica et Cosmochimica Acta 95, 196-212.

1314   Caricchi, L., Simpson, G., Schaltegger, U., 2014. Zircons reveal magma fluxes in the Earth's crust. Nature 511,
1315   457–461.

1316   Catlos, E.J., Gilley, L.D. Harrison, T.M., 2002. Interpretation of monazite ages obtained via in situ analysis.
1317   Chem. Geol. 188, 193-215.

1318   Charlier, B.L.A., Wilson, C.J.N., 2010. Chronology and evolution of caldera-forming and post-caldera magma
1319   systems at Okataina Volcano, New Zealand from zircon U-Th model-age spectra. J. Petrol. 51, 1121-1141.

1320   Charlier, B.L.A., Peate, D.W., Wilson, C.J.N., Lowenstern, J.B., Storey, M. Brown, S.J.A., 2003. Crystallisation
1321   ages in coeval silicic magma bodies; ^{238}U- ^{230}Th disequilibrium evidence from the Rotoiti and Earthquake
1322   Flat eruption deposits, Taupo volcanic zone, New Zealand. Earth Planet. Sci. Lett. 206, 441-457.

1323   Charlier, B.L.A., Wilson, C.J.N., Lowenstern, J.B., Blake, S., van Calsteren, P.W. Davidson, J.P., 2005. Magma
1324   generation at a large, hyperactive silicic volcano (Taupo, New Zealand) revealed by U-Th and U-Pb
1325   systematics in zircons. . J. Petrol. 46, 3-32.

1326   Cheng, H., Edwards, L.R., Shen, C.C., Polyak, V.J., Asmerom, Y., Woodhead, J., Hellstrom, J., Wang, Y.,
1327   Kong, X., Spötl, C., Wang, X., 2013. Improvements in ^{230}Th dating, ^{230}Th and ^{234}U half-life values, and U–
1328   Th isotopic measurements by multi-collector inductively coupled plasma mass spectrometry. Earth and
1329   Planetary Science Letters 371, 82-91.

1330   Chew, D.M., Petrus, J.A., Kamber, B.S., 2014. U–Pb LA–ICPMS dating using accessory mineral standards with
1331   variable common Pb. Chem. Geol. 363, 185-199.

1332   Chew, D. M., Sylvester, P. J., Tubrett, M. N., 2011. U–Pb and Th–Pb dating of apatite by LA-ICPMS. Chem.
1333   Geol. 280, 200–216.

1334   Chiaradia, M., Schaltegger, U., Spikings, R., 2013. How Accurately Can We Date the Duration of Magmatic-
1335   Hydrothermal Events in Porphyry Systems?—An Invited Paper. Econ. Geol. 108, 565-584.

1336   Claiborne, L.L., Miller, C.F., Flanagan, D M., Clynne, M A., Wooden, J.L., 2010. Zircon reveals protracted
1337   magma storage and recycling beneath Mount St. Helens. Geology 38, 1011–1014.

1338   Compston, W., Williams, I.S. Meyer, C.E., 1984. U-Pb geochronology of zircons from lunar breccia 73217
1339   using a sensitive high mass-resolution ion microprobe. J. Geophys. Res. 89, Suppl.(B), 525-534.

1340   Condon, D.J., 2005. Progress report on the U-Pb interlaboratory experiment. Geochim. Cosmochim. Acta,
1341   Suppl., 69, 319.

1342   Condon, D.J., McLean, N., Noble, S.R., Bowring, S.A., 2010. Isotopic composition (238U/235U) of some
1343   commonly used uranium reference materials. Geochim. Cosmochim. Acta 74, 7127–7143.

1344   Condon, D. J., Schoene, B., McLean, N. M., Bowring, S., Parrish, R. R. Metrology and Traceability of U-Pb
1345   Isotope Dilution Geochronology (EARTHTIME Tracer Calibration Part I). Geochim. Cosmochim. Acta, in
1346   review.

1347   Cooper, K.M., Kent, A.J.R., 2014. Rapid remobilization of magmatic crystals kept in cold storage. Nature 506,
1348   480-485.

1349   Cottle, J.M., Horstwood, M.S.A. Parrish, R.R., 2009. A new approach to single shot laser ablation analysis and
1350   its application to in situ Pb/U geochronology. J. Anal. Atom. Spectrom. 24, 1355-1363.

1351 Cottle, J.M., Kylander-Clark, A.R., Vrijmoed, J.C., 2012. U–Th/Pb geochronology of detrital zircon and
1352   monazite by single shot laser ablation inductively coupled plasma mass spectrometry (SS-LA-ICPMS).
1353   Chem. Geol. 332–333 (2012) 136–147

1354 Crowley, J., Schoene, B., Bowring, S., 2007. U-Pb dating of zircon in the Bishop Tuff at the millennial scale.
1355   Geology 35, 1123.

1356 Crowley, Q.G., Heron, K., Riggs, N., Kamber, B., Chew, D., McConnell, B., Benn, K., 2014. Chemical
1357   Abrasion Applied to LA-ICP-MS U–Pb Zircon Geochronology. Minerals 4, 503-518.

1358 D'Abzac, F.-X., Seydoux-Guillaume, A.-M., Chmeleff, J., Datas, L., Poitrasson, F., 2011. Study of near infra
1359   red femtosecond laser induced particles using transmission electron microscopy and low pressure impaction:
1360   Implications for laser ablation–inductively coupled plasma-mass spectrometry analysis of natural monazite,
1361   Spectrochim. Acta Part B: Atomic Spectroscopy, 66, 671-680.

1362 Danišík, M., Shane, P., Schmitt, A.K., Hogg, A., Santos, G.M., Storm, S., Evans, N., Fifield, K, Lindsay, J.M.,
1363   2012. Re-anchoring the late Pleistocene tephrochronology of New Zealand based on concordant radiocarbon
1364   ages and combined ^{238}U/^{230}Th disequilibrium and (U-Th)/He zircon ages. Earth and Planetary Science
1365   Letters 349, 240-250.

1366 Dalrymple, G.B., Grove, M., Lovera, O.M., Harrison, T.M., Hulen, J.B., Lanphere, M.A., 1999. Age and
1367   thermal history of the Geysers plutonic complex (felsite unit), Geysers geothermal field, California: a
1368 ^{40}Ar/^{39}Ar and U-Pb study. Earth and Planetary Science Letters 173(3), 285-298.

1369 Davis, D.W., Amelin, Y., Nowell, G.M., Parrish, R.R., 2005. Hf isotopes in zircon from the western Superior
1370   province, Canada: Implications for Archean crustal development and evolution of the depleted mantle
1371   reservoir. Precambrian Res. 140, 132–156.

1372 Dickinson, W.R., Gehrels, G.E., 2009. Use of U–Pb ages of detrital zircons to infer maximum depositional ages
1373   of strata: A test against a Colorado Plateau Mesozoic database. Earth Planet. Sci. Lett. 288, 115-125.

1374 Dobrzhinetskaya, L., Wirth, R., Green, H., 2014. Diamonds in Earth's oldest zircons from Jack Hills
1375   conglomerate, Australia, are contamination. Earth Planet. Sci. Lett. 387, 212-218.

1376 Feng, R., Machado, N. Ludden, J., 1993. Lead geochronology of zircon by laserprobe-inductively coupled
1377   plasma mass spectrometry (LP-ICPMS). Geochim. Cosmochim. Acta 57, 3479–3486

1378 Fletcher, I.R., McNaughton, N.J., Davis, W.J. Rasmussen, B., 2010. Matrix effects and calibration limitations in
1379   ion probe U/Pb and Th/Pb dating of monazite. Chem. Geol. 270, 31-44.

1380 Foster, G., Parrish, R.R., Horstwood, M.S., Chenery, S., Pyle, J., Gibson, H.D., 2004. The generation of
1381   prograde P-T-t points and paths; a textural, compositional, and chronological study of metamorphic
1382   monazite. Earth and Planetary Science Letters 228(1), 125-142.

1383 Frei, D., Gerdes, A., 2009. Precise and accurate in situ U–Pb dating of zircon with high sample throughput by
1384   automated LA-SF-ICP-MS. Chem. Geol. 261, 261–270.

1385 Fryer, B.J., Jackson, S.E. Longerich, H.P., 1993. The application of laser ablation microprobe-inductively
1386   coupled plasma-mass spectrometry (LAM-ICP-MS) to in situ (U)-Pb geochronology. Chem. Geol. 109, 1-8.

1387 Gehrels, G.E., Valencia, V.A. Ruiz, J., 2008. Enhanced precision, accuracy, efficiency, and spatial resolution of
1388   U-Pb ages by laser ablation–multicollector–inductively coupled plasma-mass spectrometry, Geochem.
1389   Geophys. Geosyst. 9, Q03017, doi:10.1029/2007GC001805.

1390 Gerdes, A., Zeh, A., 2009. Zircon formation versus zircon alteration—new insights from combined U–Pb and
1391   Lu–Hf in-situ LA-ICP-MS analyses, and consequences for the interpretation of Archean zircon from the
1392   Central Zone of the Limpopo Belt. Chem. Geol. 261, 230-243.

1393 Gerstenberger, H., Haase, G., 1997. A highly effective emitter substance for mass spectrometric Pb isotope ratio
1394   determinations. Chem. Geol. 136, 309–312.

1395 Goudie, D.J., Fisher, C.M., Hanchar, J.M., Crowley, J.L. Ayers, J.C., 2014. Simultaneous in situ determination
1396   of U-Pb and Sm-Nd isotopes in monazite by laser ablation ICP-MS. Geochem. Geophys. Geosyst. 15, 2575-
1397   2600, doi:10.1002/2014GC005431.

1398 Grange, M.L., Pidgeon, R.T., Nemchin, A.A., Timms, N.E., Meyer, C., 2013. Interpreting U–Pb data from
1399   primary and secondary features in lunar zircon. Geochim. Cosmochim. Acta 101, 112–132.

1400 Guex, J., Schoene, B., Bartolini, A., Spangenberg, J., Schaltegger, U., O'Dogherty, L., Taylor, D., Bucher, H.,
1401   Atudorei, V., 2012. Geochronological constraints on post-extinction recovery of the ammonoids and carbon
1402   cycle perturbations during the Early Jurassic. Palaeogeogr. Palaeoclimat. Palaeoecol. 346-347, 1–11.

1403 Guillong, M., Horn, I., Günther, D. 2003. A comparison of 266nm, 213nm and 193nm produced from a single
1404   solid state Nd:YAG laser for laser ablation ICP-MS. J. Anal. At. Spectrom., 18, 1224-1230.

1405 Hanchar, J.M., 2009. Results from a round-robin study assessing the precision and accuracy of LA-ICPMS
1406   U/Pb geochronology of zircon. Eos Trans. AGU, 90, Fall Meet. Suppl., Abs.: V53B-04

1407 Harrison, T.M., McKeegan, K.D., LeFort, P. 1995 Detection of inherited monazite in the Manaslu leucogranite
1408   by ^{208}Pb/^{232}Th ion microprobe dating: Crystallization age and tectonic implications. Earth Planet. Sci. Letts.,
1409   133, Issues 3–4, 271–282.

1410 Harrison, T.M., Schmitt, A.K., 2007. High sensitivity mapping of Ti distributions in Hadean zircons. Earth
1411   Planet. Sci. Lett. 261, 9-19.

1412 Hellebrand, E., Moeller, A., Whitehouse, M. Cannat, M., 2007. Formation of oceanic zircons. Geochim.
1413   Cosmochim. Acta 71, A391.

1414 Hietpas, J., Samson, S., Moecher, D. Schmitt, A.K., 2010. Recovering tectonic events from the sedimentary
1415   record; detrital monazite plays in high fidelity. Geology 38, 167-170.

1416 Hiess, J., Condon, D. J., McLean, N., Noble, S. R., 2012. ^{238}U/^{235}U Systematics in Terrestrial Uranium-Bearing
1417   Minerals. Science 335, 1610–1610.

1418 Hofmann, A.E., Valley, J.W., Watson, E.B., Cavosie, A.J. Eiler, J.M., 2009. Sub-micron scale distributions of
1419   trace elements in zircon. Contrib. Mineral. Petrol. 158, 317-335.

1420 Holden, P., Lanc, P., Ireland, T. R., Harrison, T. M., Foster, J. J., Bruce, Z., 2009. Mass-spectrometric mining of
1421   Hadean zircons by automated SHRIMP multi-collector and single-collector U/Pb zircon age dating: The first
1422   100,000 grains. International Journal of Mass Spectrometry, 286(2), 53-63.

1423 Horn, I., von Blanckenburg, F. 2007. Investigation on elemental and isotopic fractionation during 196 nm
1424   femtosecond laser ablation multiple collector inductively coupled plasma mass spectrometry. Spectrochim.
1425   Acta B, 62, issue 4, 410-422.

1426 Hunter, J.L., 2009. Improving Depth Profile Measurements of Natural Materials: Lessons Learned from
1427   Electronic Materials Depth-Profiling, in: Fayek, M. (Ed.), Secondary Ion Mass Spectrometry in the Earth
1428   Sciences: Gleaning the Big Picture from a Small Spot. Short Course Series. Mineral. Assoc. Canada (MAC),
1429   Québec, 133-148.

1430 Huyskens, M. H., Iizuka, T., Amelin, Y., 2012. Evaluation of colloidal silicagels for lead isotopic measurements

1431   using thermal ionisation mass spectrometry. J. Anal. Atom. Spectrom. 27, 1439-1446.

1432 Ickert, R.B., Hiess, J., Williams, I.S., Holden, P., Ireland, T.R., Lanc, P., Schram, N., Foster, J.J. Clement, S.W.,

1433   2008. Determining high precision, in situ, oxygen isotope ratios with a SHRIMP II; analyses of MPI-DING

1434   silicate-glass reference materials and zircon from contrasting granites. Chem. Geol. 257, 114-128.

1435 Ireland, T.R., Williams, I.S., 2003. Considerations in zircon geochronology by SIMS. Rev. Mineral. Geochem.

1436   53, 215-241.

1437 Jackson, S., Pearson, N., Griffin, W., Belousova, E., 2004. The application of laser ablation-inductively coupled

1438   plasma-mass spectrometry to in situ U–Pb zircon geochronology. Chem. Geol. 211, 47–69.

1439 Janots, E., Berger, A., Gnos, E., Whitehouse, M., Lewin, E., Pettke, T., 2012. Constraints on fluid evolution

1440   during metamorphism from U–Th–Pb systematics in Alpine hydrothermal monazite. Chem. Geol. 326, 61-

1441   71.

1442 Jeon, H., Whitehouse, M. J. (2014). A Critical Evaluation of U–Pb Calibration Schemes Used in SIMS Zircon

1443   Geochronology. Geostandards and Geoanalytical Research. DOI: 10.1111/j.1751-908X.2014.00325.x

1444 Johnston, S., Gehrels, G., Valencia, V., Ruiz, J., 2009. Small volume U-Pb zircon geochronology by laser

1445   ablation-multicollector-ICP-MS. Chem. Geol. 259, 218–229.

1446 Kalsbeek, F., 1992. The statistical distribution of the mean squared weighted deviation—comment: Isochrons,

1447   errorchrons, and the use of MSWD-values. Chem. Geol. 94, 241-242.

1448 Kennedy A.K., Wotzlaw J.F., Crowley J., Schmitz M. Schaltegger U., 2014. Eocene reference material for

1449   microanalysis of U-Th-Pb isotopes and trace elements. Can. Mineral. 52, in press.

1450 Klemetti, E.W., Deering, C.D., Cooper, K.M. Roeske, S.M., 2011. Magmatic perturbations in the Okataina

1451   Volcanic Complex, New Zealand at thousand-year timescales recorded in single zircon crystals. Earth

1452   Planet. Sci. Lett. 305, 185-194.

1453 Koch, J., Wälle, M., Pisonero, J., Günther, D., 2006. Performance characteristics of ultra-violet femtosecond

1454   laser ablation inductively coupled plasma mass spectrometry at ~265 and ~200 nm. J. Analyt. Atom.

1455   Spectrom. 21, 932-940.

1456 Koch, J., Günther, D., 2011. Review of the state-of-the-art of laser ablation inductively coupled plasma mass

1457   spectrometry. Appl. Spectroscopy 65, 155A-162A.

1458 Kooijman, E., Mezger, K., Berndt, J., 2010. Constraints on the U-Pb systematics of metamorphic rutile from in-

1459   situ LA-ICP-MS analysis. Earth Planet. Sci Letts, 293, 321-330

1460 Kooijman, E., Berndt, J., Mezger, K., 2012. U-Pb dating of zircon by laser ablation ICP-MS: recent

1461   improvements and new insights. European J. Mineral. 24, 5-21.

1462 Koornneef, J.M., Dorta, L., Hattendorf, B., Fontaine, G.H., Bourdon, B., Stracke, A., Ulmer, P., Günther D.,

1463   2012. *In situ* analysis of ^{230}Th–^{232}Th–^{238}U ratios in titanite by fs-LA-MC-ICPMS. J. Anal. At. Spectrom. 27,

1464   1863-1874.

1465 Košler, J., Tubrett, M.N., Sylvester, P.J., 2001. Application of Laser Ablation ICP-MS to U-Th-Pb Dating of

1466   Monazite. Geostand. Newsletters 25, 375-386.

1467 Košler, J., Sláma, J., Belousova, E., Corfu, F., Gehrels, G. E., Gerdes, A., Horstwood, M.S.A., Sircombe, K.N.,

1468   Sylvester, P.J., Tiepolo, M., Whitehouse, M.J., Woodhead, J.D., 2013. U-Pb detrital zircon analysis - results

1469   of an inter-laboratory comparison. Geostand. Geoanal. Res. 37, 243–259.

1470 Krogh, T.E., 1982. Improved accuracy of U–Pb zircon ages by the creation of more concordant systems using

1471   an air abrasion technique. Geochim. Cosmochim. Acta 46, 637–649.

1472 Kryza, R., Crowley, Q.G., Larionov, A., Pin, C., Oberc-Dziedzic, T. Mochnacka, K., 2012. Chemical abrasion

1473   applied to SHRIMP zircon geochronology: An example from the Variscan Karkonosze Granite (Sudetes,

1474   SW Poland). Gondwana Res. 21, 757-767.

1475 Kusiak, M.A., Whitehouse, M.J., Wilde, S.A., Nemchin, A.A., Clark, C., 2013. Mobilization of radiogenic Pb in

1476   zircon revealed by ion imaging: Implications for early Earth geochronology. Geology 41, 291–294.

1477 Kylander-Clark, A.R.C., Hacker, B.R., Cottle, J.M., 2013. Laser-ablation split-stream ICP petrochronology,

1478   Chem. Geol. 345, Pages 99-112

1479 Li, Q.L., Li, X.H., Liu, Y., Tang, G.Q., Yang, J.H., Zhu, W.G., 2010. Precise U-Pb and Pb-Pb dating of

1480   Phanerozoic baddeleyite by SIMS with oxygen flooding technique. J. Anal. Atom. Spectrom. 25, 1107-1113.

1481 Ludwig, K.R., 2003. Isoplot 3.00 A Geochronological toolkit for Microsoft Excel. Berkeley Geochron. Center

1482   Spec. Publ. 4, 71 pp.

1483 Machado, N., Gauthier, G., 1996. Determination of 207Pb/206Pb ages on zircon and monazite by laser-ablation

1484   ICPMS and application to a study of sedimentary provenance and metamorphism in southeastern Brazil.

1485   Geochim. Cosmochim. Acta, 60, 5063-5073.

1486 Mahon, K.I., 1996. The New "York" regression: Application of an improved statistical method to geochemistry.

1487   International Geology Review 38(4), 293-303.

1488 Marillo-Sialer, E., Woodhead, J., Hergt, J., Greig, A., Guillong, M., Gleadow, A., Evans., N., Paton, C., 2014.

1489   The zircon 'matrix effect': evidence for an ablation rate control on the accuracy of U–Pb age determinations

1490   by LA-ICP-MS. J. Anal. At. Spectrom. 29, 981-989.

1491 Mattinson, J., 2005. Zircon U–Pb chemical abrasion ("CA-TIMS") method: combined annealing and multi-step

1492   partial dissolution analysis for improved precision and accuracy of zircon ages. Chem. Geol. 220, 47–66.

1493 Mattinson, J.M., 2010. Analysis of the relative decay constants of ^{235}U and ^{238}U by multi-step CA-TIMS

1494   measurements of closed-system natural zircon samples. Chem. Geol. 275, 186–198.

1495 Mays, C.W., Atherton, D.R., Lloyd, R.D., Lucas, H.F., Stover, B.J., Bruenger, F.W., 1962. The half-period of

1496   Ra 228 (Mesothorium)", Utah Univ. Report, COO-225, 92-105.

1497 McLean, N.M., Amelin Y.V., Bowring, S.A., 2011a. Quantification of mass independent fractionation in Pb by

1498   TIMS and implications for U-Pb geochronology. Abstract V33G-05, Fall Meeting, AGU, San Francisco,

1499   Calif., 5-9 Dec. 2011.

1500 McLean, N.M., Bowring, J.F., Bowring, S.A., 2011b. An algorithm for U-Pb isotope dilution data reduction and

1501   uncertainty propagation. Geochem. Geophys. Geosyst. 12, Q0AA18. doi:10.1029/2010GC003478

1502 Miller, J., Matzel, J., Miller, C., Burgess, S., Miller, R., 2007. Zircon growth and recycling during the assembly

1503   of large, composite arc plutons. J. Volcanol. Geotherm. Res. 167, 282–299.

1504 Möller, A., O'Brien, P.J., Kennedy, A. Kröner, A., 2003. Linking growth episodes of zircon and metamorphic

1505   textures to zircon chemistry; an example from the ultrahigh-temperature granulites of Rogaland, SW

1506   Norway. Geol. Soc. London, Spec. Publ. 220, 65-81.

1507 Moser, D.E., Davis, W.J., Reddy, S.M., Flemming, R.L. Hart, R.J., 2009. Zircon U-Pb strain chronometry

1508   reveals deep impact-triggered flow. Earth Planet. Sci. Lett. 277, 73-79.

1509 Müller, W., Shelley, M., Miller, P., Broude, S., 2009. Initial performance metrics of a new custom-designed ArF
1510   excimer LA-ICPMS system coupled to a two-volume laser-ablation cell. J. Analyt. Atom. Spectrom. 24,
1511   209-214.

1512 Murray, K.K., Boyd, R.K., Eberlin, M.N., Langley, G.J., Li, L. and Naito, T. 2013. Definition of terms relating
1513   to mass spectrometry (IUPAC recommendations 2013). Pure Appl. Chem., 85, 1515-1609.

1514 Paces, J. B., Miller, J. D., 1993. Precise U-Pb Ages of Duluth Complex and Related Mafic Intrusions,
1515   Northeastern Minnesota - Geochronological Insights to Physical, Petrogenetic, Paleomagnetic, and
1516   Tectonomagmatic Processes Associated with the 1.1 Ga Midcontinent Rift System. J. Geophys. Res. 98(B8),
1517   13997–14013.

1518 Palacz, Z., Jones, T., Tootel, D., Guest, R., Locke, S., 2011. Peformance characteristics of an enhanced Daly ion
1519   counting system for TIMS. Min. Mag. 75, 1588.

1520 Parrish, R.R., Noble, S., 2003. Zircon U-Th-Pb geochronology by isotope dilution - thermal ionization mass
1521   spectrometry (ID-TIMS), in: Hanchar, J.M., Koskin, P.O.W. (eds.) Rircon. Rev. Mineral. Geochem. 53, 183-
1522   213.

1523 Parrish, R.R., Gough, S.J., Searle, M.P., Waters, D.J., 2006. Plate velocity exhumation of ultrahigh-pressure
1524   eclogites in the Pakistan Himalaya. Geology, 34, 989-992.

1525 Peres, P., Kita, N.T., Valley, J.W., Fernandes, F. and Schuhmacher, M., 2012. New sample holder geometry for
1526   high precision isotope analyses. Surface and Interface Analysis 45(1), 553-556.

1527 Peterman E.M., Mattinson, J.M. Hacker B.R. 2012. Multi-step TIMS and CA-TIMS monazite U–Pb
1528   geochronology. Chem. Geol. 312-313, 58–73.

1529 Pullen, A., Ibáñez-Mejía, M., Gehrels, G.E., Ibáñez-Mejía, J.C., Pecha, M., 2014. What happens when n= 1000?
1530   Creating large-n geochronological datasets with LA-ICP-MS for geologic investigations. J. Anal. At.
1531   Spectrom., 2014,29, 971-980

1532 von Quadt, A., Gallhofer, D., Guillong, M., Peytcheva, I., Waelle, M., Sakata, S., 2014. U–Pb dating of
1533   CA/non-CA treated zircons obtained by LA-ICP-MS and CA-TIMS techniques: impact for their geological
1534   interpretation. J. Anal. At. Spectrom. 29, 1618-1629.

1535 Rasmussen, B., 2005. Zircon growth in very low grade metasedimentary rocks: evidence for zirconium mobility
1536   at~ 250 C. Contrib. Mineral. Petrol. 150(2), 146-155.

1537 Rasmussen, B., Fletcher, I. R., Gregory, C. J., Muhling, J. R., Suvorova, A. A., 2011. Tranquillityite: The last
1538   lunar mineral comes down to Earth. Geology 40, 83–86.

1539 Reid, M.R., Coath, C.D., Harrison, T.M. McKeegan, K.D., 1997. Prolonged residence times for the youngest
1540   rhyolites associated with Long Valley Caldera; [230]Th-[238]U ion microprobe dating of young zircons. Earth
1541   Planet. Sci. Lett. 150, 27-39.

1542 Reid, M.R., Vazquez, J.A., Schmitt, A.K., 2011. Zircon-scale insights into the history of a Supervolcano,
1543   Bishop Tuff, Long Valley, California, with implications for the Ti-in-zircon geothermometer. Contributions
1544   to Mineralogy and Petrology 161(2), 293-311.

1545 Renne, P.R., Mundil, R., Balco, G., Min, K., Ludwig, K.R., 2010. Joint determination of 40K decay constants
1546   and 40Ar/40K for the Fish Canyon sanidine standard, and improved accuracy for 40Ar/39Ar geochronology.
1547   Geochim. Cosmochim. Acta 74, 5349–5367.

1548   Richter, S., Goldberg, S., Mason, P., Traina, A., Schwieters, J., 2001. Linearity tests for secondary electron
1549   multipliers used in isotope ratio mass spectrometry. Int. J. Mass Spectrom. 206, 105–127.

1550   Rioux, M., Bowring, S., Dudás, F., Hanson, R., 2010. Characterizing the U–Pb systematics of baddeleyite
1551   through chemical abrasion: application of multi-step digestion methods to baddeleyite geochronology.
1552   Contrib. Mineral. Petrol. 160, 777-801.

1553   Rioux, M., Lissenberg, C. J., McLean, N. M., Bowring, S. A., MacLeod, C. J., Hellebrand, E., Shimizu, N.,
1554   2012. Protracted timescales of lower crustal growth at the fast-spreading East Pacific Rise. Nature Geosci. 5,
1555   275–278.

1556   Rivera, T.A., Schmitz, M.D., Crowley J.L., Storey, M., 2014. Rapid magma evolution constrained by zircon
1557   petrochronology and $^{40}Ar/^{39}Ar$ sanidine ages for the Huckleberry Ridge Tuff, Yellowstone, USA. Geology
1558   42, 643-646.

1559   Rivera, T.A., Storey, M., Schmitz, M.D., Crowley, J.L., 2013. Age intercalibration of $^{40}Ar/^{39}Ar$ sanidine and
1560   chemically distinct U/Pb zircon populations from the Alder Creek Rhyolite Quaternary geochronology
1561   standard. Chemical Geology 345, 87-98.

1562   Robert, J., Miranda, C.F., Muxart, R., 1969. Mesure de la période du protactinium 231 par microcalorimétrie.
1563   Radiochimca Acta 11(2), 104-108.

1564   Romer, R.L., 2003. Alpha-recoil in U-Pb geochronology: effective sample size matters. Contributions to
1565   Mineralogy and Petrology 145(4), 481-491.

1566   Rubatto, D., 2002. Zircon trace element geochemistry: partitioning with garnet and the link between U-Pb ages
1567   and metamorphism. Chem. Geol. 184, 123-138.

1568   Rubatto, D., Hermann, J., 2007. Experimental zircon/melt and zircon/garnet trace element partitioning and
1569   implications for the geochronology of crustal rocks. Chem. Geol. 241, 38–61.

1570   Russo, R. E., Mao, X., Gonzalez, J. J., Zorba, V., Yoo, J., 2013. Laser ablation in analytical chemistry. Analyt.
1571   Chem. 85, 6162-6177.

1572   Sanudo-Wilhelmy, S.A., Flegal, A.R., 1994. Temporal Variations in Lead Concentrations and Isotopic
1573   Composition in the Southern California Bight. Geochim. Cosmochim. Acta 58, 3315-3320.

1574   Schärer, U., 1984. The effect of initial ^{230}Th disequilibrium on young U-Pb ages; the Makalu case, Himalaya.
1575   Earth Planet. Sci. Lett. 67, 191-204.

1576   Schaltegger, U., Brack, P., Ovtcharova, M., Peytcheva, I., Schoene, B., Stracke, A., Marocchi, M., Bargossi,
1577   G.M., 2009. Zircon and titanite recording 1.5 million years of magma accretion, crystallization and initial
1578   cooling in a composite pluton (southern Adamello batholith, northern Italy). Earth Planet. Sci. Lett. 286,
1579   208–218.

1580   Schmitt, A. K., 2011. Uranium Series Accessory Crystal Dating of Magmatic Processes. Ann. Rev. Earth
1581   Planet. Sci. 39, 321–349.

1582   Schmitt, A.K., Zack, T., 2012. High-sensitivity U–Pb rutile dating by secondary ion mass spectrometry (SIMS)
1583   with an O_2^+ primary beam. Chemical Geology 332, 65-73.

1584   Schmitt, A.K., Chamberlain, K.R., Swapp, S.M., Harrison, T.M.,2010. In situ U-Pb dating of micro-baddeleyite
1585   by secondary ion mass spectrometry. Chemical Geology 269(3), 386-395.

1586 Schmitz, M., Bowring, S., 2001. U-Pb zircon and titanite systematics of the Fish Canyon Tuff: an assessment of

1587   high-precision U-Pb geochronology and its application to young volcanic rocks. Geochim. Cosmochim.

1588   Acta 65, 2571–2587.

1589 Schoene, B., 2014. U–Th–Pb Geochronology. The Crust (2nd ed., Vol. 4, pp. 341–378). Elsevier Ltd.

1590 Schoene, B., Condon, D.J., Morgan, L., McLean, N., 2013. Precision and accuracy in Geochronology. Elements

1591   9, 19-24

1592 Schoene, B., Crowley, J., Condon, D., Schmitz, M., Bowring, S., 2006. Reassessing the uranium decay

1593   constants for geochronology using ID-TIMS U–Pb data. Geochim. Cosmochim. Acta 70, 426–445.

1594 Schoene, B., Guex, J., Bartolini, A., Schaltegger, U., Blackburn, T. J., 2010a. Correlating the end-Triassic mass

1595   extinction and flood basalt volcanism at the 100 ka level. Geology 38, 387–390.

1596 Schoene, B., Latkoczy, C., Schaltegger, U., Günther, D., 2010b. A new method integrating high-precision U–Pb

1597   geochronology with zircon trace element analysis (U–Pb TIMS-TEA). Geochim. Cosmochim. Acta 74,

1598   7144–7159.

1599 Schoene, B., Schaltegger, U., Brack, P., Latkoczy, C., Stracke, A., Günther, D., 2012. Rates of magma

1600   differentiation and emplacement in a ballooning pluton recorded by U–Pb TIMS-TEA, Adamello batholith,

1601   Italy. Earth Planet. Sci. Lett. 355-356, 162–173.

1602 Schumacher, M., De Chambost, E., McKeegan, K.D., Harrison, T.M., Migeon, H., 1994. In situ dating of zircon

1603   with the CAMECA ims 1270 Secondary Ion Mass Spectrometry, in: Benninghoven, A., Werner, H.W.,

1604   Shimizu, R., Nihei, Y. (eds.), SIMS. IX. John Wiley & Sons, pp. 919-922.

1605 Shaheen, M. E., Gagnon, J. E., Fryer, B. J., 2012. Femtosecond (fs) lasers coupled with modern ICP-MS

1606   instruments provide new and improved potential for in situ elemental and isotopic analyses in the

1607   geosciences. Chem. Geol. 330-331, 260–273.

1608 Shane, P., Storm, S., Schmitt, A.K., Lindsay, J.M., 2012. Timing and conditions of formation of granitoid clasts

1609   erupted in recent pyroclastic deposits from Tarawera Volcano (New Zealand). Lithos 140-141, 1-10.

1610 Simon, J.I., Reid, M.R., 2005. The pace of rhyolite differentiation and storage in an "archetypical" silicic

1611   magma system, Long Valley, California. Earth Planet. Sci. Lett. 235, 123-140.

1612 Sláma, J., Košler, J., Condon, D.J., Crowley, J.L., Gerdes, A., Hanchar J.M., Horstwood, M.S.A., Morris, G.A.,

1613   Nasdala, L., Norberg, N., Schaltegger, U., Schoene, B., Tubrett, M.N., Whitehouse, M.J., 2008. Plešovice

1614   zircon – a new natural reference material for U-Pb and Hf isotopic microanalysis. Chem. Geol. 249, 1-35.

1615 Spencer, K.J., Hacker, B.R., Kylander-Clark, A.R.C., Andersen, T.B., Cottle, J.M., Stearns, M.A., Poletti, J.E.,

1616   Seward, G.G.E., 2013. Campaign-style titanite U–Pb dating by laser-ablation ICP: Implications for crustal

1617   flow, phase transformations and titanite closure, Chem. Geol. 341, 84-101.

1618 Stacey, J.S., Kramers, J.D., 1975. Approximation of terrestrial lead isotope evolution by a two-stage model.

1619   Earth Planet. Sci. Lett. 26, 207-221.

1620 Steely, A.N., Hourigan, J.K., Juel, E., 2014. Discrete multi-pulse laser ablation depth profiling with a single-

1621   collector ICP-MS: Sub-micron U–Pb geochronology of zircon and the effect of radiation damage on depth-

1622   dependent fractionation, Chem. Geol. 372, Pages 92-108.

1623 Stelten, M.E., Cooper, K.M., Vazquez, J.A., Reid, M.R., Barfod, G.H., Wimpenny, J., Yin, Q.Z., 2013. Magma

1624   mixing and the generation of isotopically juvenile silicic magma at Yellowstone caldera inferred from

1625   coupling ^{238}U-^{230}Th ages with trace elements and Hf and O isotopes in zircon and Pb isotopes in sanidine.

1626   Contributions to Mineralogy and Petrology 166(2), 587-613.

1627 Stern, R.A., Amelin, Y., 2003. Assessment of errors in SIMS zircon U-Pb geochronology using a natural zircon

1628   standard and NIST SRM 610 glass. Chem. Geol. 197, 111-142.

1629 Stern, R.A., Bodorkos, S., Kamo, S.L., Hickman, A.H., Corfu, F., 2009. Measurement of SIMS instrumental

1630   mass fractionation of Pb isotopes during zircon dating. Geostand. Geoanalyt. Res. 33, 145-168.

1631 Storey, C.D., Jeffries, T.E., Smith, M., 2006. Common lead-corrected laser ablation ICP–MS U–Pb systematics

1632   and geochronology of titanite, Chem. Geol. 227, 37-52.

1633 Storm, S., Shane, P., Schmitt, A.K., Lindsay, J.M., 2011. Contrasting punctuated zircon growth in two syn-

1634   erupted rhyolite magmas from Tarawera volcano: Insights to crystal diversity in magmatic systems. Earth

1635   Planet. Sci. Lett. 301, 511-520.

1636 Storm, S., Shane, P., Schmitt, A.K., Lindsay, J.M., 2012. Decoupled crystallization and eruption histories of the

1637   rhyolite magmatic system at Tarawera Volcano revealed by zircon ages and growth rates. Contrib. Mineral.

1638   Petrol. 163, 505-519.

1639 Storm, S., Schmitt, A.K., Shane, P., Lindsay, J.M., 2014. Zircon trace element chemistry at sub-micrometer

1640   resolution for Tarawera volcano, New Zealand, and implications for rhyolite magma evolution. Contrib.

1641   Mineral. Petrol. 67, 1-19.

1642 Taylor, R., Clark, C. Reddy, S.M., 2012. The effect of grain orientation on secondary ion mass spectrometry

1643   (SIMS) analysis of rutile. Chem. Geol. 300, 81-87.

1644 Thomson, S.N., Gehrels, G.E., Ruiz, J., Buchwaldt, R., 2012. Routine low-damage apatite U-Pb dating using

1645   laser ablation-multicollector-ICPMS. Geochemistry Geophysics Geosystems 13, Issue 2,

1646 Valley, J. W., Cavosie, A. J., Ushikubo, T., Reinhard, D. A., Lawrence, D. F., Larson, D. J., et al. (2014).

1647   Hadean age for a post-magma-ocean zircon confirmed by atom-probe tomography. Nature Geosci. 7, 219–

1648   223.

1649 Vazquez, J.A., Reid, M.R., 2004. Probing the accumulation history of the voluminous Toba magma. Science

1650   305, 991-994.

1651 Vorhies, S.H., Ague, J.J., Schmitt, A.K. (2013). Zircon growth and recrystallization during progressive

1652   metamorphism, Barrovian zones, Scotland. American Mineralogist 98(1), 219-230.

1653 Watt, G.R., Griffin, B.J., Kinny, P.D., 2000. Charge contrast imaging of geological materials in the

1654   environmental scanning electron microscope. American Mineralogist 85, 1784–1794.

1655 Watson, E.B., 1996. Dissolution, growth and survival of zircons during crustal fusion; kinetic principles,

1656   geological models and implications for isotopic inheritance. Geol. Soc. America, Spec. Pap. 315, 43-56.

1657 Watson, E. B., Harrison, T. M., 1983. Zircon saturation revisited: temperature and composition effects in a

1658   variety of crustal magma types. Earth Planet. Sci.Lett. 64, 295–304.

1659 Wendt, I., Carl, C., 1991. The statistical distribution of the mean squared weighted deviation. Chem. Geol., Isot.

1660   Geosci. Sect. 86, 275–285.

1661 White, L.T., Ireland, T.R., 2012. High uranium matrix effect in zircon and its implications for SHRIMP U/Pb

1662   age determinations. Chem. Geol. 306-307, 78-91.

1663 Wiedenbeck, M., Allé, P., Corfu, F., Griffin, W., Meier, M., Oberli, F., von Quadt, A., Roddick, J.C., Spiegel,

1664   W., 1995. Three natural zircon standards for U-Th-Pb, Lu-Hf, trace element and REE analyses. Geostand.

1665   Newslett. 19, 1–23.

1666 Wingate, M.T.D., Compston, W., 2000. Crystal orientation effects during ion microprobe U-Pb analysis of

1667   baddeleyite. Chem. Geol. 168, 75-97.

1668 Wotzlaw J.-F., Schaltegger U., Frick D.A., Dungan M.A., Gerdes A., Günther D., 2013. Tracking the evolution

1669   of large volume silicic magma reservoirs from assembly to supereruption. Geology 41, 867-870.

1670 Wotzlaw J.F., Hüsing S.K., Hilgen F.J., Schaltegger U., 2014. Testing the gold standard of geochronology

1671   against astronomical time: High-precision U-Pb geochronology of orbitally tuned ash beds from the

1672   Mediterranean Miocene. Earth Planet. Sci. Lett. 407, 19-34

1673 Zack, T., Stockli, D.F., Luvizotto, G.L., Barth, M.G., Belousova, E., Wolfe, M.R., Hinton, R.W., 2011. In situ

1674   U–Pb rutile dating by LA-ICP-MS: [208]Pb correction and prospects for geological applications. Contributions

1675   to Mineralogy and Petrology 162(3), 515-530.

1676 Zeh, A., Ovtcharova, M., Wilson, A.H., Schaltegger, U., 2015. The Bushveld Complex was emplaced and

1677   cooled in less than one million years - results from zirconology and tectonic implications. Earth Planet. Sci.

1678   Lett., in press.

1679

1680

1681 **Figures:**

1682 Fig. 1: Concordia diagram of two c. 7.24-7.26 Ma old zircons showing the effect of different

1683   corrections during the CA-ID-TIMS procedure on the precision and the accuracy of the

1684   result; the grey band describes the uncertainty of the position of the concordia curve

1685   due to the decay constant uncertainties. a) effect of common-Pb correction: blue

1686   ellipses: zircon with $Pb_{rad}/Pb_{com} = 21.0$; red ellipses: zircon with $Pb_{rad}/Pb_{com} = 6.7$.

1687   Three ellipses are shown with different Pb_{com} isotope compositions from left to right

1688 $^{206}Pb/^{204}Pb = 18.70, 18.45, 18.20$, respectively, and $^{207}Pb/^{204}Pb = 15.75, 15.60, 15.45$,

1689   respectively; the Pb_{com} isotope composition does not significantly influence the

1690 $^{206}Pb/^{238}U$, but does affect the $^{207}Pb/^{235}U$.

1691   (b) same two zircons as above, before (below the concordia) and after (concordant)

1692   correction for initial ^{230}Th disequilibrium (Schärer 1984) using $D_{Th/U} = 0.16$ to calculate

1693   Th/U$_{source}$. The corrected uncertainty ellipses contain 50% uncertainty of the Th/U$_{source}$,

1694   propagated onto the final date after McLean et al. (2011). Example from Wotzlaw et al.

1695   (2014; zircons MDC7_z6 and z10).

1696 Fig. 2: Compilation of all R33 reference zircon data (Black et al 2004) from the University of

1697   Geneva isotope laboratory, measured between 2004 and 2014 with different tracer

1698   solutions and different mass spectrometers equipped with different secondary electron

1699   multipliers (SEM's). The period 2004-2006 contains data measured on MAT262 at

1700   ETH Zürich (ETP-SEM) and TRITON at UNIGE (MasCom1-SEM), with a ^{205}Pb-^{235}U

1701   tracer; data measured during the period 2007-2011 used an Earthtime (ET) ^{205}Pb-^{233}U-

1702 ^{235}U tracer, measured on a Triton with a MasCom-2 SEM; the data from 2012-2014

1703   were measured with an ET ^{202}Pb-^{205}Pb-^{233}U-^{235}U tracer on a Triton with a MasCom3-

1704   SEM.

1705   Fig. 3: Standard SIMS sample holder geometry for the CAMECA ims1270/1280 showing

1706 ^{206}Pb/^{238}U ages determined on fragments of reference zircon z6266 mounted on mount

1707   IP222 (Stern and Amelin, 2003). The random distribution indicates the absence of bias

1708   relative to the position within the sample mount (XY-effect) when targets are located

1709   within the 15 mm "bullseye" of the mount; XY effects close to the window edge are

1710   particularly problematic for high-precision stable isotope analyses, and are mitigated by

1711   large sample holder designs (Peres et al., 2012). (B) Histogram and relative probability

1712   for ^{206}Pb/^{238}U ages in (A) indicating the reproducibility for a linear Pb/U RSF vs.

1713   UO$^+$/U$^+$ calibration based on analysis of reference zircon z6266 using the University of

1714   California Los Angeles (UCLA) CAMECA ims1270. Average sputter rate for this

1715   experiment is indicated in μm^3/s/nA O$^-$.

1716   Fig. 4: Schematic of the UCLA CAMECA ims1270 large magnet radius ion microprobe (A)

1717   with types of quantitative SIMS analysis used in geochronology: spot mode (B; CL

1718   image with typical spot dimensions overlain), depth profiling (C; surface map of

1719   unsectioned zircon with SIMS crater on prism face), scanning ion imaging SII (D;

1720 ^{49}Ti$^+$/SiO$^+$ secondary ion maps overlain onto a Hadean zircon surface image showing

1721   high-Ti domains in red associated with fractures), and direct ion imaging DII using the

1722   ims1270 channel plate (E; ^{90}Zr$^+$ secondary ion distribution of a zircon with a quartz

1723   inclusion in the center of the image; image generated from an accumulated channel

1724   plate signal; white square indicates outline of the field aperture).

1725   Fig. 5: Apparent ^{206}Pb/^{238}U date vs. U abundance for zircons from Tasmanian dolerites

1726   analysed by SHRIMP RG (A; White and Ireland, 2012) and CAMECA ims1270 at

1727   UCLA (B) relative to the Temora reference zircon. The legend shows the range of the

1728   calibration parameter UO$^+$/U$^+$ relative to Temora. Gray dashed hockey-stick line

1729   schematically represents unbiased low-U analyses in agreement with other radiometric

1730   age determinations for Tasmanian dolerite of ~175 Ma and the apparent age increase at

1731   U >2500 ppm (after Fig. 1 in White and Ireland, 2012).

1732   Fig. 6: Probability density distribution (PDD) curves of U-Th zircon crystallization ages for

1733   four sequential rhyolite eruptions from Tarawera volcano (Taupo volcanic zone, New

1734   Zealand). Model ages are based on two point isochrons using zircon and melt (from

1735   whole-rock analysis) compositions. Numbers of individual crystal face, interior (after

1736   grinding to ~15 μm depth), and core (in equatorial section at ~50 μm depth) dates are

1737   indicated for each curve. Eruption ages (horizontal bars with volcano symbol) are based

1738   on ^{14}C ages. Interior ages linked to rim ages of the preceding eruption indicate high

1739   probabilities (P = 0.10 - 0.54) of similarity suggesting consecutive overgrowth.

1740   Horizontal arrows indicate the time lapse Δt between major peaks in rim and interior

1741   age distributions, translating into integrated growth rates of ~10^{-13} to 10^{-15} cm/s. Note

1742   that not only the population, but also individual zircon crystals can record episodic

1743   crystallization over time-spans >10^5 a. Data from Storm et al. (2011) and Klemetti et al.

1744   (2011).

1745   Fig. 7: Age and compositional zonation revealed by depth-profiling of Kaharoa zircon (grain

1746   KaT2z3 in Storm et al., 2011; 2014). Parallel depth profiles were acquired on

1747   unpolished crystal faces (A); the side opposite to the analyzed crystal face was

1748   sectioned to ~15 μm depth and imaged by CL (B). U-Th age and U concentration depth

1749   profiles (C); Ti concentrations with model Ti-in-zircon temperatures using aTiO_2 = 0.5

1750   and aSiO_2 = 1 (D); and Zr/Hf as indicator for temperature-dependent zircon

1751   fractionation (E). The excursion to high-T (and more primitive melt compositions

1752   indicated by low U and high Zr/Hf) after ca. 45 ka is interpreted as local rejuvenation

1753   of the crystal storage reservoir following the Rotoiti caldera-forming eruption which

1754   was followed by the eruption of comparatively hot and primitive intra-caldera

1755   rhyodacites (see Storm et al., 2014, for references).

1756   Fig. 8: Examples of age-ranked ^{206}Pb/^{238}U dates showing different degrees of age dispersion

1757   (data from Broderick, 2014). a) sample with statistically significant age cluster (MSWD

1758   = 1.6, within the range of acceptable values for N=10; Wendt and Carl 1991) and 2

1759   xeno- or antecrystic zircons with ~250 ka older age ; b) sample showing a larger age

1760   dispersion over 184 ± 83 ka; the probability density distribution (PDD) curve indicates

1761   two major phases of zircon crystallization at ~42.6 and ~42.5 Ma; c) set of 9 ^{206}Pb/^{238}U

1762   dates indicating an age scatter over 205 ± 86 ka, showing an additional peak of zircon

1763   crystallization at ~42.45 Ma.

1764   Fig. 9: (a) EBSD (left) and U-Pb data (right) from a ductile zircon crystal from a lower

1765   crustal mafic mylonite xenolith, illustrating the role of structural state on U-Pb

1766   concordance. The central axis of the crystal has experienced complete resetting of the

1767   U-Pb chronometer after deformation resulting in up to 35º rotation of the crystal lattice.

1768   Crystal is ca. 100μm across (Figures from Moser et al., 2009, reproduced with

1769   permission from Elsevier Science). (b) CCI (left) and BSE (right) images of a dolostone

1770   from the Bunter Formation, North Sea. The CCI image shows dolomite cores with

1771   evidence of partial dissolution surrounded by new concentric growth material. This

1772   illustrates the ability of CCI to resolve complexity in crystal structures aiding targeting

1773   for high spatial resolution in-situ analysis. Scale bar in both images is 100μm. Images

1774   courtesy of Jeremy Rushton, BGS, for the Bunter Properties Project.

1775   Fig. 10: In-situ analysis of micro-zircons from a Northern Madison Range (Montana)

1776   metamorphic mafic dike. (A) Micro-zircon crystals in backscatter-image showing

1777   crystals completely enclosed in quartz (z272), intersected by an annealed fracture in

1778   quartz (z271), and interstitial at grain boundaries between quartz and garnet (z274).

1779   Inset illustrates primary beam spot size (~20 μm) and dimensions of field aperture (~10

1780   μm) limiting secondary ion acceptance. (B) Concordia diagram of SIMS analyses

1781   highlighting spots in (A). Discordance is high for crystals located at grain boundaries,

1782   whereas those hosted in intact quartz are concordant. These results suggest that

1783   radiation damage alone is insufficient to explain discordant vs. concordant behaviour of

1784   zircon, and indicates that shielding can mitigate Pb-loss (Ault et al., 2012).

1785   Fig. 11: SIMS depth profile for zircon from the sillimanite-K-feldspar zone sample 286B

1786   (Glen Muick, Barrovian, Scotland). (A) ^{206}Pb/^{238}U dates and percent concordance

1787   between ^{207}Pb/^{235}U and ^{206}Pb/^{238}U dates and (B) Th/U. (C) backscatter electron image

1788   of depth-profiled zircon (with SIMS analysis spots in center of crystal showing up as

1789   bright areas due to charging where the conductive Au coat has been removed). The

1790   analyzed metamorphic overgrowth is only ~1.5 μm thick and is preceded by a spike in

1791   Th/U interpreted to be due to Th mobilization during partial melting. Crystal interior is

1792   an inherited core, likely of metamorphic origin (Vorhies et al., 2013)

1793   Fig. 12: (a) Model using middle and heavy rare earth element variations in ID-TIMS dated

1794   zircon as a result of titanite fractionation, used to calculate percentage of crystal in the

1795   crystallizing Fish Canyon Tuff magma over 420 ka; (b) modelled compositional trends

1796   for a titanite-free fractionation assemblage (grey points) and for an assemblage

1797   containing 0.4% titanite. The model documents near-solidification with 78% crystals at

1798   28.4 Ma and subsequent rejuvenation of the magma to 40% crystals at 28.2 Ma

1799   (modified from Wotzlaw et al., 2013).

1800

1801 **Tables**

1802   Tab. 1: Charted strengths and weaknesses of the three methods of U-Pb dating. Sources: [1]

1803   Schmitt et al. (2010), [2] Frei and Gerdes (2009), [3] Cottle et al. (2009)

1804   Tab. 2: Natural zircon reference materials characterized by ID-TIMS; source of data: [1]

1805   Kennedy et al. (2014); [2] Sláma et al. (2008); [3] Black et al. (2003); [4] Black et al.

1806   (2004); [5] Jackson et al. (2004); [6] Schaltegger et al., unpubl., in: Boekhout et al.

1807   (2012); [7] Wiedenbeck et al. (1995); [8] Schoene et al., (2006); [9] Paces and Miller

1808   (1993). Uncertainties are indicated in X/Y format (following Schoene et al., 2006)

1809   where available. Data in [1], [2], [6] and [8] are corrected for initial ^{230}Th

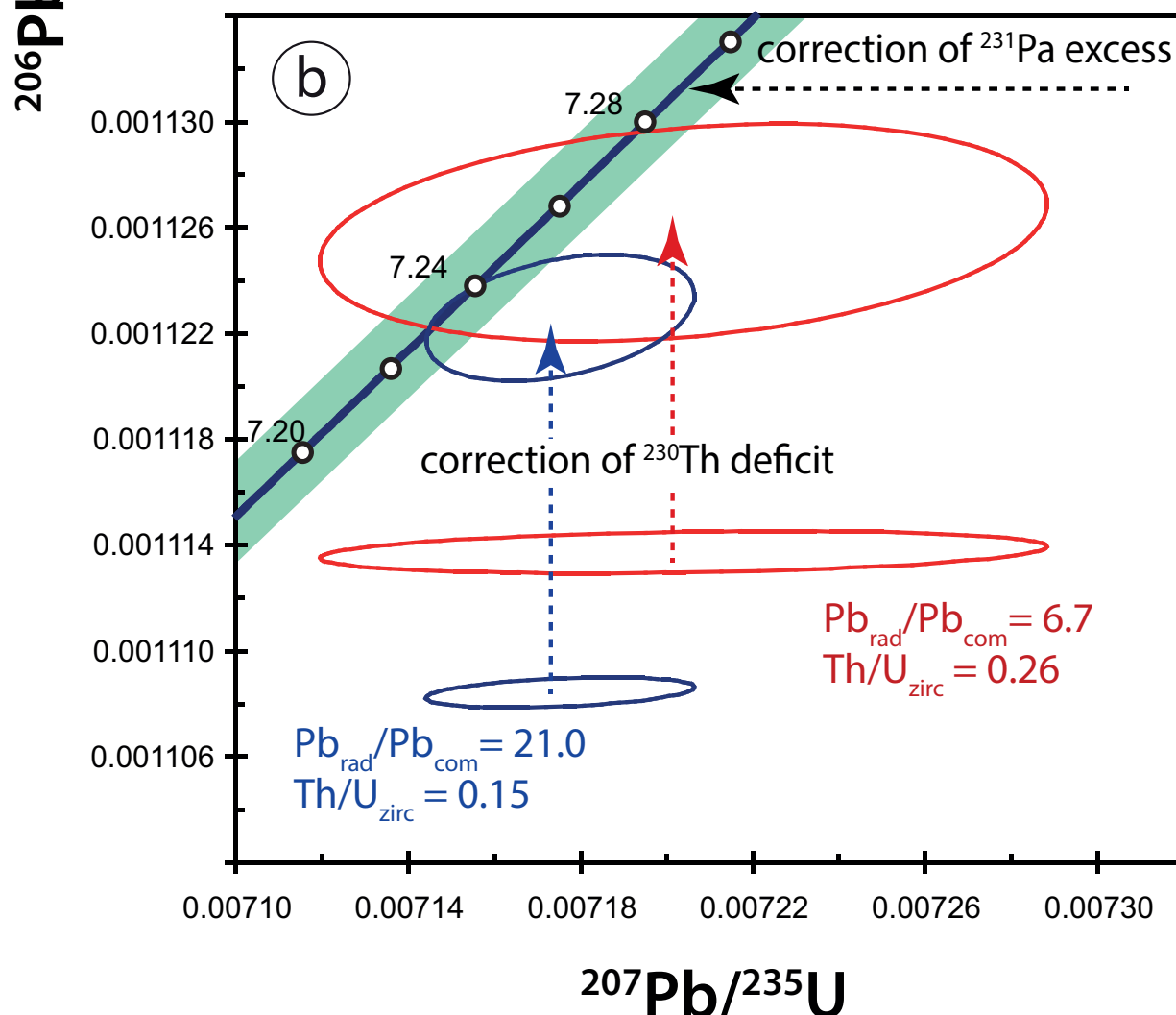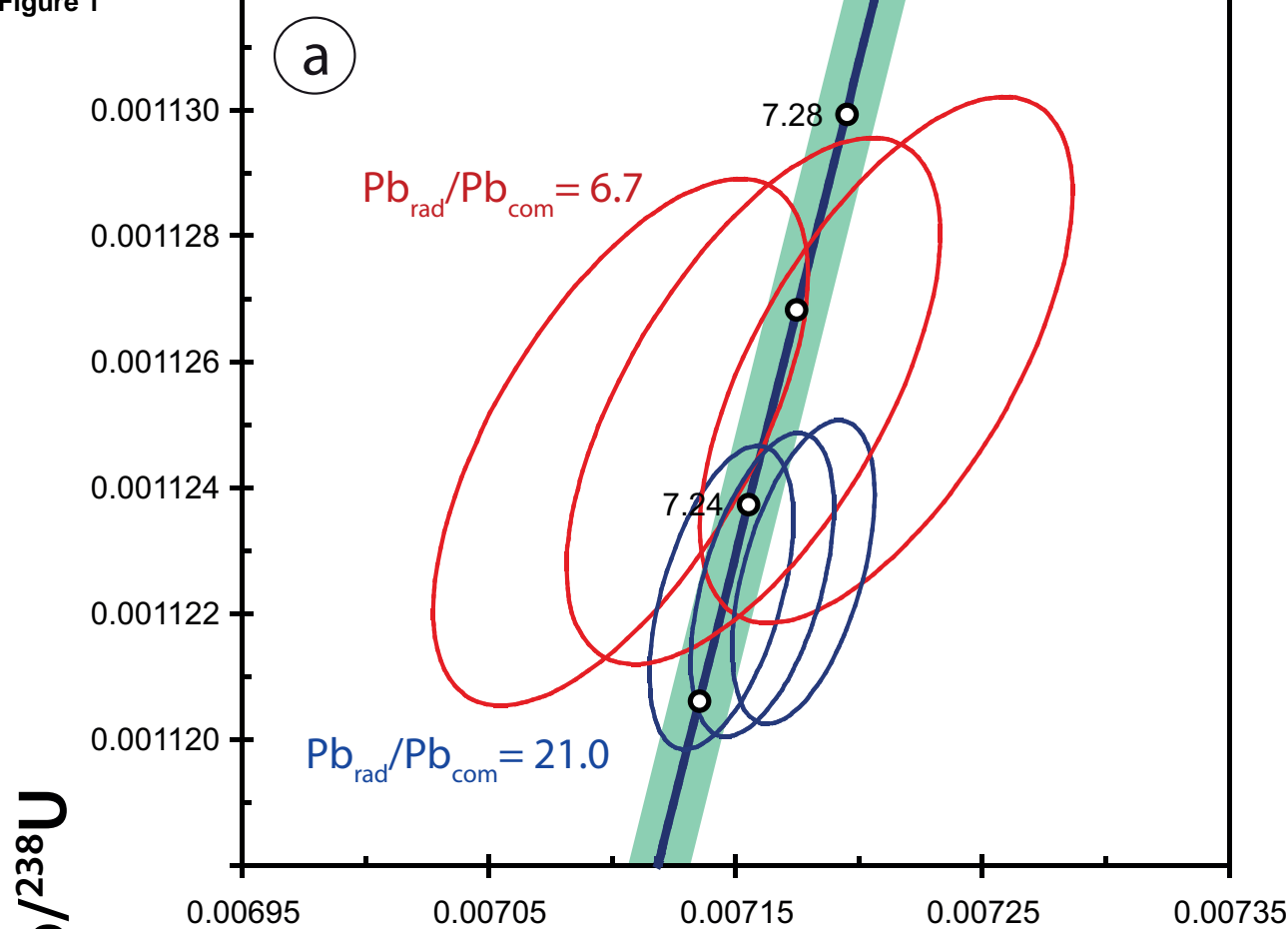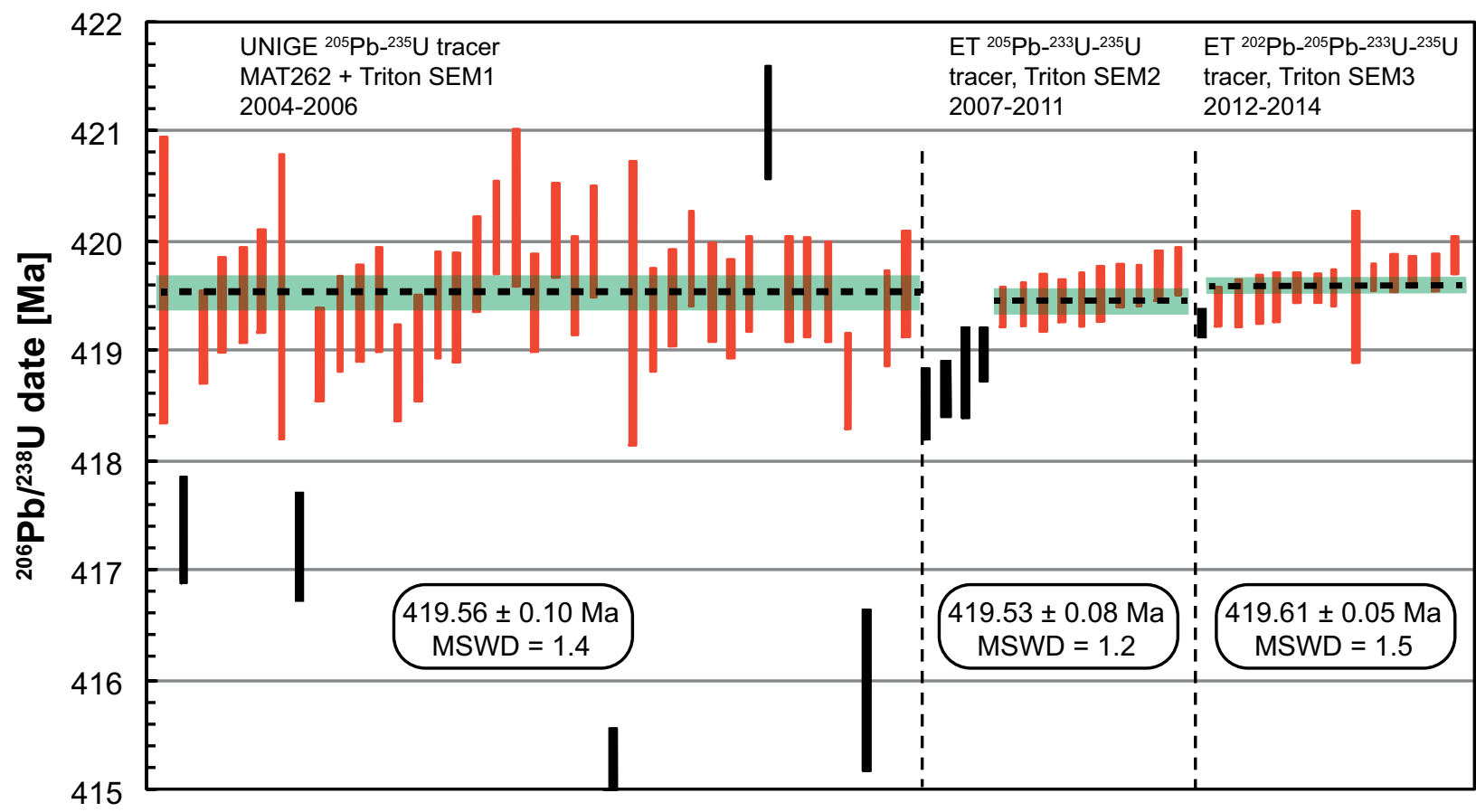1810   disequilibrium.

1811

1812

Figure 1

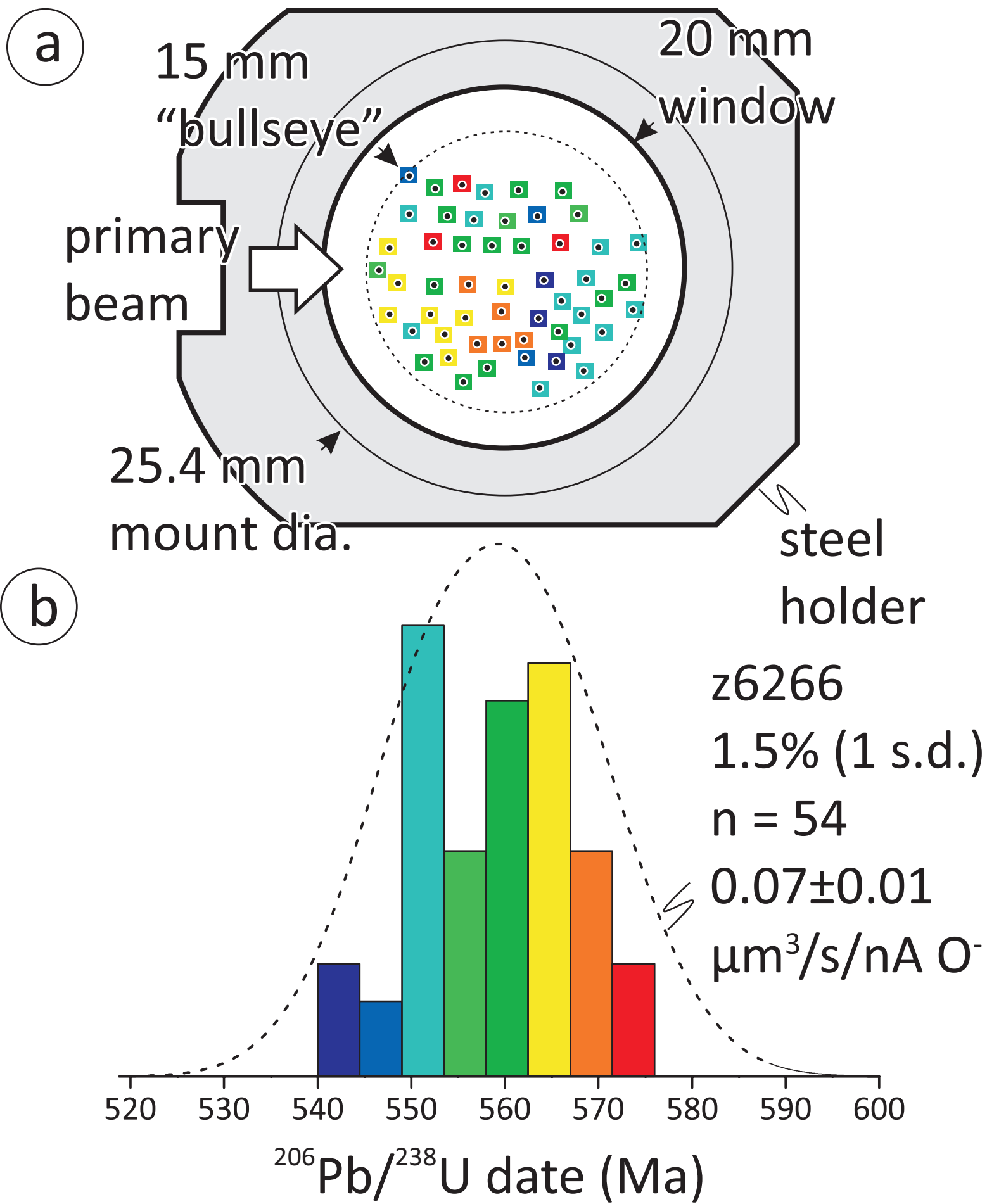**Figure 2**

UNIGE ^{205}Pb-^{235}U tracer
MAT262 + Triton SEM1
2004-2006

ET ^{205}Pb-^{233}U-^{235}U
tracer, Triton SEM2
2007-2011

ET ^{202}Pb-^{205}Pb-^{233}U-^{235}U
tracer, Triton SEM3
2012-2014

419.56 ± 0.10 Ma
MSWD = 1.4

419.53 ± 0.08 Ma
MSWD = 1.2

419.61 ± 0.05 Ma
MSWD = 1.5

^{206}Pb/^{238}U date [Ma]

Figure 3

a — 15 mm "bullseye", 20 mm window, primary beam, 25.4 mm mount dia., steel holder

b — z6266, 1.5% (1 s.d.), n = 54, 0.07±0.01 μm^3/s/nA O$^-$

^{206}Pb/^{238}U date (Ma)

Figure 4

a

Secondary column

Primary column

Magnet

Field aperture

Ga source

~1 m

Sample chamber

Detection

Channel plate

b 31 ka

595 Ma

25 μm

c intensity

depth

50 μm

d

2 μm

e

← 20 μm →

spot   depth profile   SII   DII

Figure 5

a

Tasmanian dolerite
SHRIMP RG - Test2a
White and Ireland (2012)

<5.4	5.6	5.8	6.0	6.2	6.4	>6.4

UO^+/U^+

Temora range

b

Tasmanian dolerite
CAMECA ims1270

<7.6	7.7	7.8	7.9	8.0	8.1	>8.2

UO^+/U^+

Temora range

$^{206}Pb/^{238}U$ date (Ma)

U (ppm)

Figure 6

relative probability

Kaharoa 0.7 ka
faces 62[a]
interiors 61[a]
cores 67[b]

[a]Storm et al. (2011)
[b]Klemetti et al. (2011)

faces   interiors   cores

0.10

Waiohau 13.7 ka
faces 29[a]
interiors 29[a]

0.32

Rerewhakaaitu 17.7 ka
faces 62[a]
interiors 59[a]

0.54

Okareka 21.9 ka
faces 61[a]
interiors 60[a]

0   10   20   40   60   80   100   150   200   300   s.e.

U-Th zircon model age (ka)

Figure 7

Figure 8

a

$^{206}Pb/^{238}U$ date:
42.511 ± 0.081 Ma
MSWD = 1.6, n = 10

Δt_{zrc}=93 ± 60 ka

– Dt –

b

Δt_{zrc}=184 ± 83 ka

——— Dt ———

c

Δt_{zrc}=205 ± 86 ka

——— Dt ———

Ma

42.2   42.3   42.4   42.5   42.6   42.7   42.8   42.9

$^{206}Pb/^{238}U$ date

Figure 9

Figure 10

(a) annealed fracture / Quartz / 30 μm / z271 / z272 / z274 / field aperture / spot / Garnet

(b) N Madison Range (Montana) metamorphosed mafic dike

zircons in (A)
other zircons

1800
1400
1000
600
~1750 Ma regional metamorphism
z272 0%
z271 7%
z274 57%
1σ error ellipses and % discordance
~75 Ma contact metamorphism

$^{206}Pb/^{238}U$

$^{207}Pb/^{235}U$

Ault et al. (2012)

Figure 11

Vorhies et al. (2013)

Figure 12

Panel a: vol.% crystals (top axis: 40, 45, 55, 65, 75, 85) vs $^{206}Pb/^{238}U$ date (left axis: 28.6, 28.4, 28.2)

40% crystals @ 28.62Ma — 1

76% crystals @ 28.40 Ma — 2

45% crystals @ 28.20 Ma — 3

Panel b: Dy (ppm) (100, 200, 300, 400, 500) vs Yb/Dy (2, 4, 6, 8)

Fractionating assemblage contains
- 0.4 % titanite
- no titanite

50%

10%

10%

40% crystals @ 28.62Ma — 1 3

50%

70%

76% crystals @ 28.40 Ma — 2

45% crystals @ 28.20 Ma

Tab. 1

	ID-TIMS	**SIMS**	**LA-ICP-MS**
Absolute age resolution (2σ)	U-Pb high to very high: ≤0.1% precision and accuracy	U-Th and U-Pb ca. 1-2 %; very high (~10^3-10^4 years) for U-Th dating <300 ka	U-Pb ca. 2% Th-Pb ca. 3%
Spatial resolution	Poor (mixing of age domains in single crystals hardly avoidable)	Excellent (sub-µm in depth profiling); quasi non-destructive	Good (20-30µm laterally, single µm vertically, depending on analytical system)
Useful yield for U	<1% (as UO_2^+)	0.7-1% (as UO^+)	Very variable (0.01-2.8%) depending on type of mass spec*)
Uuseful yield for Pb	High (~5%), depending on the source of Si-gel	High (~1%) [1]	Intermediate (~0.2%-0.4%) to high (2%) depending on type of mass spec [2]*)
Time requirements for sample preparation and analysis	Slow (digestion and chemical separation)	Fast (CL imagery, volumetric excavation rate ~0.1 μm^3/sec/nA primary beam) [1]	Very fast (CL imagery, volumetric excavation rate ~0.125 μm^3/pulse at 2.4 J cm^{-3} fluence) [3]
Preferred geologic applicability	Volcanic and plutonic systems of any age	Young volcanic systems with volcanic and plutonic enclaves; Metamorphic systems; Microcrystal and in situ analysis	Detrital provenance studies, young volcanic and plutonic systems, metam-orphic systems, in situ analysis

*) Useful yields in % (=ions detected/total number of atoms in sample volume for a species of interest) for U and Pb, respectively; for quadrupole-ICP-MS: 0.01%, 0.01%; for single collector, sector-field ICP-MS: 0.3%, 0.2%; for multicollector ICP-MS: 0.4-2.8%, 0.3-2%.

Tab. 2

Name	Certified age [Ma]	Type of age	Source
AUSZ2	$38.8963 \pm 0.0044/0.012$	$^{206}Pb/^{238}U$	[1]
Plešovice	$337.13 \pm 0.06/0.23$	$^{206}Pb/^{238}U$	[2]
Temora 1	416.75 ± 0.24	$^{206}Pb/^{238}U$	[3]
Temora 2	416.78 ± 0.33	$^{206}Pb/^{238}U$	[4]
R33	418.9 ± 0.4	$^{206}Pb/^{238}U$	[4]
	419.26 ± 0.39	$^{206}Pb/^{238}U$	[4]
GJ-1	608.53 ± 0.37	$^{207}Pb/^{206}Pb$	[5]
GJ-1 nr. 67	600.5 ± 0.4	$^{206}Pb/^{238}U$	[6]
Harvard 91500	1065.4 ± 0.3	$^{207}Pb/^{206}Pb$	[7]
	$1066.4 \pm 0.3/5.0$	$^{207}Pb/^{206}Pb$	[8]
	$1063.6 \pm 0.2/0.3$	$^{206}Pb/^{238}U$	[8]
AS3	1099.1 ± 0.5	$^{207}Pb/^{206}Pb$	[9]
	1099.0 ± 0.7	$^{206}Pb/^{238}U$	[9]
	$1098.6 \pm 0.3/5.0$	$^{207}Pb/^{206}Pb$	[8]
	$1095.9 \pm 0.2/0.3$	$^{206}Pb/^{238}U$	[8]
FC1	1099.0 ± 0.6	$^{207}Pb/^{206}Pb$	[9]
	1099.9 ± 1.1	$^{206}Pb/^{238}U$	[9]
QGNG	1851.5 ± 0.3	$^{207}Pb/^{206}Pb$	[8]
	$1848.7 \pm 0.7/0.9$	$^{206}Pb/^{238}U$	[8]